Palaeogeography, Palaeoclimatology, Palaeoecology 441 (2016) 627–652

Contents lists available at ScienceDirect

Palaeogeography, Palaeoclimatology, Palaeoecology

journal homepage: www.elsevier.com/locate/palaeo

Palaeoclimatic and site-specific conditions in the early Permian fossil forest of Chemnitz—Sedimentological, geochemical and palaeobotanical evidence

Ludwig Luthardt [a,*], Ronny Rößler [a], Joerg W. Schneider [b,c]

[a] Museum für Naturkunde Chemnitz, Moritzstraße 20, D-09111 Chemnitz, Germany
[b] Geological Institute, Technische Universität Bergakademie Freiberg, Bernhard-von-Cotta-Straße 2, D-09599 Freiberg, Germany
[c] Kazan Federal University, 18 Kremlevskaya Str., Kazan 420008, Russian Federation

ARTICLE INFO

Article history:
Received 5 August 2015
Received in revised form 13 October 2015
Accepted 15 October 2015
Available online 26 October 2015

Keywords:
Fossil forest
T^0 assemblage
Palaeosol
Root systems
Seasonality
Precipitation

ABSTRACT

As significant indicators of deep-time palaeoclimate, a number of new palaeontological, pedological and geochemical characteristics are provided for the Chemnitz Fossil Lagerstätte to depict more precisely its environmental conditions. For the first time, several lines of evidence indicate that this fossil forest, instantaneously preserved by volcanic deposits, once received an annual precipitation of around 800–1100 mm, but grew on a nearly unweathered palaeosol. Although the composition of this rich and diverse T^0 assemblage suggests a hygrophilous, dense and multi-aged vegetation dominated by conservative lineages, the habitat was affected by environmental disturbances and pronounced seasonality. Repeated changes in local moisture availability are suggested by geochemical proxies, the co-occurrence to intergrowth of calcic and ferric glaebules in the palaeosol and developmental traits of perennial vegetational elements. Specific substrate adaptation is reflected by different root systems and cyclic growth interruptions recorded in the stems, branches and roots of long-lived woody plants. Many differentially adapted terrestrial animals complete the more comprehensive reconstruction of a late Sakmarian ecosystem and its climatic and preservational controls. Albeit spatially confined, this diverse *in-situ* record may contribute to understand wetland–dryland dynamics of sub-tropical Northern Hemisphere Pangaea.

1. Introduction

The most important witness of how ancient ecosystems react to climatic and environmental changes lies in the geological record. Of overall significance in this regard are fossil forests, especially if they represent *in-situ* records that reflect not only plant remains but also diverse animals, interactions between organisms and environmental characteristics. However, significant examples of such instantaneously preserved ecosystems are rare in the late Palaeozoic. Nevertheless, if thoroughly studied and understood they can provide a detailed picture of ancient living communities in the continental realm, and offer a high potential for understanding palaeoecological relationships (Césari et al., 2012; Gastaldo et al., 2004; Hinz et al., 2010; Opluštil et al., 2014; Wang et al., 2012). An ideal example with both a long study history (Cotta, 1832; Frenzel, 1759; Sterzel, 1875) and multi-focus ongoing research (Dietrich et al., 2013; Dunlop and Rößler, 2013; Feng et al., 2012; Matysová et al., 2010; Rößler et al., 2012a,b) is the Petrified Forest of Chemnitz. It represents an early Permian (latest Sakmarian) forest ecosystem developed on a distal braidplain and buried instantaneously by the deposition of volcanic ashes and flows. The rapid coverage by pyroclastics, due to a series of explosive volcanic eruptions, led to a three-dimensional record of the forest in growth position including its palaeosol, which classifies it as an outstanding T^0 assemblage (compare characteristics given in DiMichele and Falcon-Lang, 2011).

Historically, this fossil Lagerstätte has been well known since at least the early 18th century, due to prospecting activities for precious minerals. Although there exist some scientific descriptions from that time (Frenzel, 1759), the major motivation for collecting petrifactions was the utilisation as gemstones. The interest in its palaeobotanical significance has risen since the 19th century and continues today (e.g., Barthel, 1976; Cotta, 1832; Rößler, 2000, 2006; Sterzel, 1904). However, for a long time scientific descriptions were based on coincidental finds only, which occurred during construction works in the city of Chemnitz. On the basis of such material, research on specific fern or calamitean taxa has been carried out (Feng et al., 2012; Rößler, 2000; Rößler and Galtier, 2002a, b; Rößler and Noll, 2006, 2007, 2010). Additionally, during the last two decades geological research improved the general understanding of the basin development, its facies architecture, stratigraphic subdivision and interregional correlation (Eulenberger et al., 1995; Fischer, 1991; Schneider et al., 2012).

* Corresponding author.
E-mail addresses: luthardt@mailserver.tu-freiberg.de (L. Luthardt), roessler@naturkunde-chemnitz.de (R. Rößler), schneidj@geo.tu-freiberg.de (J.W. Schneider).

http://dx.doi.org/10.1016/j.palaeo.2015.10.015
0031-0182/

Between 2008 and 2011, a scientific excavation site at Chemnitz–Hilbersdorf delivered for the first time a more complete insight into a local taphocoenosis of this fossil forest. During this excavation, a vast amount of data was gathered offering potential for a detailed, albeit spatially confined, reconstruction of this ancient forest habitat (Kretzschmar et al., 2008; Rößler et al., 2008, 2009, 2010, 2012b). The fossil record comprises a comprehensive spectrum of plant and animal remains, more complete than ever documented before. Fifty-three upright-standing petrified trees, still anchored in the original substrate, were discovered together with a variety of parautochthonously embedded stems and twigs. A countless number of leaf adpressions and moulds were found preserved in one single horizon next to various arthropod remains or reptile and amphibian skeletons exhibiting even their former body outlines (Dunlop and Rößler, 2013; Feng et al., 2014; Rößler et al., 2012b).

Within a distance of approximately 2 km from the aforementioned locality, a second excavation site in Chemnitz–Sonnenberg was initiated in 2009 and finally set up in 2014 (Rößler and Merbitz, 2009). We aim to continue this excavation during the next years to verify the knowledge about the fossil forest ecosystem, especially regarding plant and animal diversity and spatial distribution, variation of site-specific environmental characteristics within a wider area and taphonomic differences correlated with different distances from the volcano.

Other late Palaeozoic T^0 assemblages, which show similar volcanic preservational backgrounds comprise peat-forming wetland communities that flourished in the Pennsylvanian palaeoequatorial tropics, in basinal settings, obviously under long-term stable environmental and climatic conditions (Opluštil et al., 2007, 2009). However, there is a growing awareness of ice-age-caused repetitive climatic oscillations resulting in seasonal dryness and floral change even in equatorial Pangaea (DiMichele, 2014; DiMichele and Phillips, 1996; Falcon-Lang et al., 2009; Montañez and Poulsen, 2013; Pfefferkorn et al., 2008; Roscher and Schneider, 2006). In Cathaysia, conditions maintaining extended peat-forming communities, continued into to the Permian (Wang et al., 2012). On the contrary, early Permian ecosystems in Euramerica and northern Gondwana were increasingly forced by environmental and ecological dynamics (Capretz and Rohn, 2013; DiMichele et al., 2006, 2007, 2011; Galtier and Broutin, 2008; Kerp, 1996; Looy et al., 2014; Ricardi-Branco, 2008; Rößler, 2006; Tabor and Poulsen, 2008), which are documented by changing plant communities and their migration routes, changes in dominance patterns of sedimentary facies and palaeosols at different spatial and temporal scales.

In Chemnitz we have a wetland flora on mineral soil that was captured in a red-bed environment, which is commonly occupied by mesophilous to xerophilious plants (Schneider et al., 2012). This spatially restricted fossil Lagerstätte is ecologically far from the widely distributed peat-forming swamps that are most frequently documented from the Middle Pennsylvanian to the earliest Permian (e.g., DiMichele et al., 2002; Greb et al., 2003; Opluštil et al., 2009; Wagner, 1989; Wang et al., 2012). On the other hand, it has little in common with the typical extrabasinal or upland occurrences (Cridland and Morris, 1963; Falcon-Lang and Bashforth, 2004; Kerp, 1996; Pfefferkorn, 1980). This still inadequately understood occurrence of plants that usually characterise conservative peat-forming communities, show an overall absence of typical extrabasinal elements.

In order to clarify these contradictions and improve the palaeoecological model of this site we carried out additional investigations and analyses focusing on both palaeontology and geochemistry. We tried to exclude, as much as possible, any taphonomic effects that resulted from the volcanic type of entombment, which sometimes modified the preservation of fossil material. This contribution provides new results that enable us to interpret abiotic and biotic influences on the environment and to recognise some variation at the habitat spatial scale. The general aim to reconstruct this ecosystem can only be achieved by the combination of different perspectives. These include the understanding of taphonomic influences during the emplacement of pyroclastics, palaeobotanical investigations focusing on the three-dimensionally preserved plants, the appreciation of various interactions between individual organisms in the habitat, as well as local environmental constraints related to superordinated palaeoclimatic conditions. To restrain the scope of this contribution particular attention was paid to largely independent lines of evidence, which were traced by means of (1) geochemical proxies of the sedimentary basement, (2) pedogenetic features of the palaeosol, (3) the morphology, anatomy and community structure of floral elements, (4) diverse invertebrate and vertebrate animals and their mutual habitat preferences, and (5) interactions between plants, animals and microorganisms. We aim to integrate data derived from these individual lines of research in order to develop a better understanding and a more appropriate reconstruction of the whole ecosystem. This integrated approach will permit us to use this spatially constrained ecological study to understand aspects of the depositional system on a basin-wide scale, given that any small-scale site, although reflective of local conditions, also will bear a strong overprint from regional climate and sedimentary conditions.

2. Geological setting

The Petrified Forest is located in the town Chemnitz (Saxony, SE-Germany), situated in the eastern part of the early Permian Chemnitz Basin (Fig. 1A). The basin is bordered by the Granulite Massif in the North and the Erzgebirge Mountains in the South. It overlies different Carboniferous coal-bearing basin structures and metamorphic units of the Variscan basement and shows an extension of 70 × 30 km in SW–NE orientation. The basin fill consists of continental red beds and intercalated pyroclastics of early Permian (Asselian to Artinskian) and middle to late Permian (Capitanian to Wuchiapingian) age. These are overlain by late Permian (Wuchiapingian to Lopingian) marine and sabhka deposits of Zechstein Sea transgressions, as well as lowermost Triassic deposits (Legler and Schneider, 2008; Schneider et al., 2012). Up to six sedimentary megacycles can be distinguished in the continental deposits of the Chemnitz Basin, which are grouped into four formations (Fig. 2), exhibiting an overall thickness of approximately 1550 m.

2.1. Leukersdorf Formation

Representing an 800 m thick red-bed sequence of predominantly alluvial origin, the Leukersdorf Formation is characterised by three fining-up mesocycles, which are, in case of the first cycle completed by the 25 m thick lacustrine–palustrine grey sediments of the Rottluff Horizon, restricted to the eastern part of the basin, as well as by the basin-wide lacustrine Reinsdorf Carbonate Horizon (Fig. 2). There are some major pyroclastic marker horizons, e.g., the Chemnitz Tuff in the first cycle and in the third cycle the Zeisigwald Tuff, hosting the Chemnitz Fossil Forest. The dominant lithofacies type is fine-grained alluvial red beds, which interfinger with coarse clastics of semi-arid type alluvial fans from the basin margins. The ichnofauna of these “wet” red beds is dominated, and in contrast to the dry-playa red beds, characterised by infaunal burrows of the *Scoyenia* and *Planolites montanus* types (Schneider et al., 2012). Frequently, rhizolith-bearing, less mature vertic to calcic palaeosols occur, which are further diagnostic features of wet red beds (Schneider et al., 2010) The sparse floral record is restricted to minor relicts of meso- to xerophilous plants (“walchians”) typical for this kind of late Pennsylvanian to early Permian red beds.

The Reinsdorf Carbonate Horizon consists of one to five 0.30–0.50 m thick carbonate layers having a nearly basin-wide extent. The individual carbonate layers are intercalated with red-coloured fine clastics and coarse fluvial channel and sheetflood deposits of a braidplain system. The carbonates predominantly appear as homogenous micrites. In the urban area of Chemnitz they are described as laminated microbial-mat limestones and massive or partly finely laminated dolosparites, which frequently bear intraclasts and bioclasts. The microfaunal assemblage is quite diverse encompassing common gastropods and ostracods as

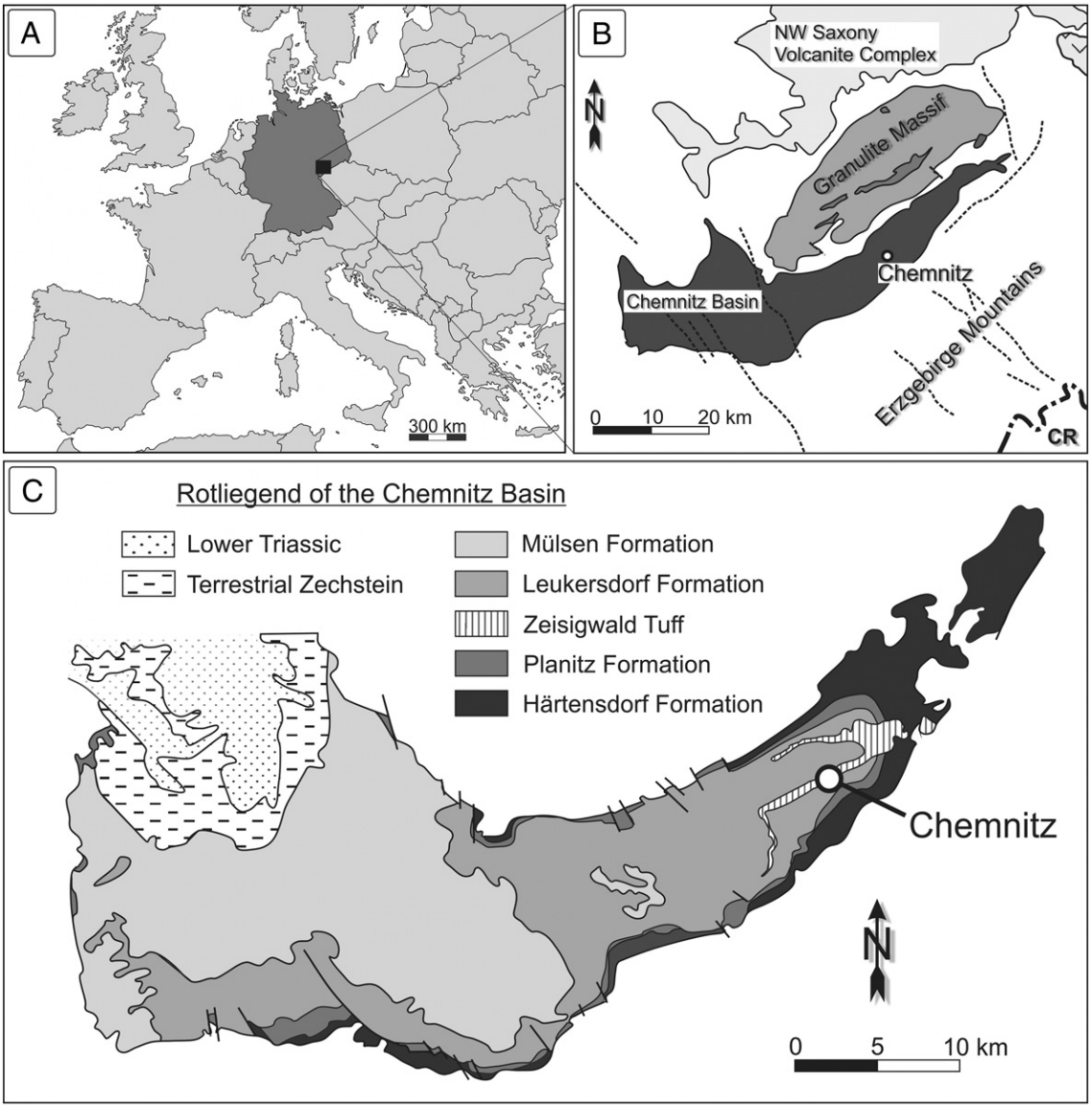

Fig. 1. (A) Geographical map. (B) Geological setting of the study area. (C) Major geological units of the Chemnitz Basin and distribution of the Zeisigwald Tuff Member; Study area is located in the town of Chemnitz. (modified from Schneider et al., 2012).

well as a few characean algae, small amphibian remains and rarely teeth of actinopterygians and xenacanthid freshwater sharks (Schneider et al., 2012). The Reinsdorf Carbonate Horizon belongs to the late Sakmarian/early Artinskian wet phase D after Roscher and Schneider (2006).

2.2. Zeisigwald Tuff—record of a short-term stacked eruption sequence

The Zeisigwald Tuff, a stratigraphic marker horizon of the Leukersdorf Formation, has been dated radiometrically at 290.6 ± 1.8 Ma, using SHRIMP U–Pb dating of zircon grains (Rößler et al., 2009). The distribution of the pyroclastic ejecta is traceable within the whole northeast of the basin (Fig. 1C) and shows a maximum thickness of about 90 m caldera fill facies and up to 55 m of caldera outflow facies in proximal position, at the northeastern margin of the city of Chemnitz (Eulenberger et al., 1995). The ejected pyroclastic material of the Zeisigwald Tuff can be detected up to a distance of approximately 10 km from the eruption centre and consists of a series of tuff layers (Fig. 3B). This pyroclastic succession is subdivided into four major units, representing successive eruption phases (Eulenberger et al., 1995; Fischer, 1991; Rößler et al., 2008).

2.3. The section at Hilbersdorf excavation site

In the middle of Chemnitz–Hilbersdorf (N 50°51′58.69″, E 12°57′32.54″) and in a proximity of around 500 m from the mapped caldera structure (Fig. 3A), the first excavation site was established by the Museum für Naturkunde Chemnitz in 2008 (Kretzschmar et al., 2008; Rößler et al., 2008, 2009, 2010, 2012b). Excavation work was done within an area of 24 × 18 m and down to a depth of 6 m below the surface. As a result, more than 2000 fossils were discovered, amongst them numerous leaf adpressions as well as petrified twigs and stems, seven vertebrate skeletons and eleven arthropod remains. In the whole excavation area 53 stems were recognised in upright position, still rooted in what we call the *in-situ* geological record of the vegetation's original substrate (Rößler et al., 2012b).

The lithological section at the excavation (Fig. 3C) was documented in detail and comprises the palaeosol horizon with the root systems of the upright-standing trees as well as the overlying basal pyroclastic units S 5 to S 3 (units b and a_1 of the eruption model presented by Eulenberger et al., 1995) of the Zeisigwald Tuff, which are eroded at the top due to recent soil-forming weathering processes.

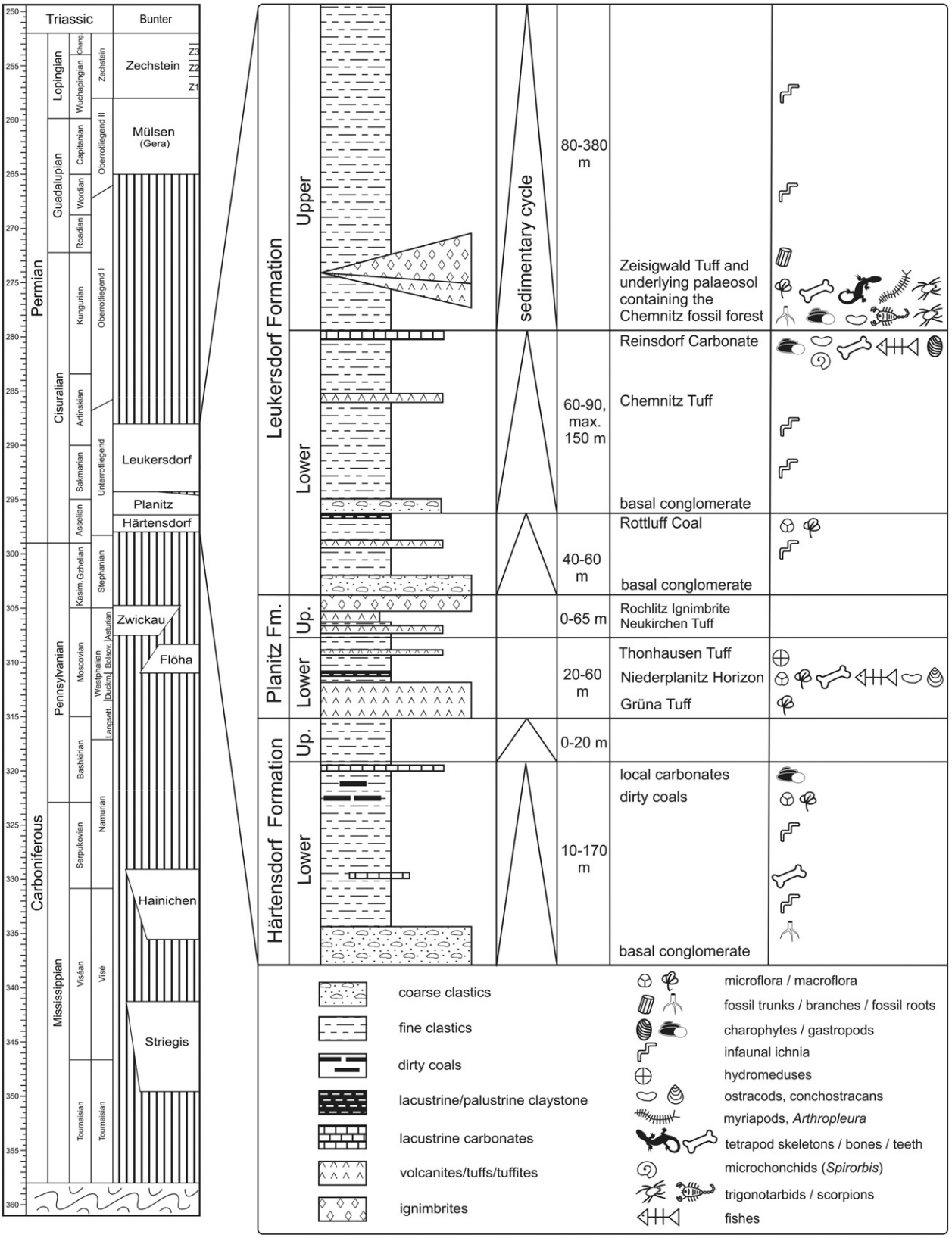

Fig. 2. Stratigraphy of the Chemnitz Basin showing the stratigraphical position of the Leukersdorf Formation and the Zeisigwald Tuff containing the Chemnitz Fossil Forest.

The 1.85 m thick palaeosol profile (Unit S 6) overlies unaltered sediments of the upper Leukersdorf Formation representing silty to fine-sandy alluvial red beds. The palaeosol profile consists of red-coloured, silty sandstone with single quartz pebbles in the upper part. In wide parts, the substrate experienced a secondary bleaching and carbonate glaebules occur (Fig. 4A). The upper part of the palaeosol horizon contains densely distributed root systems of the hygrophilous forest vegetation (Fig. 5A). On the top of the irregularly wavy palaeosol

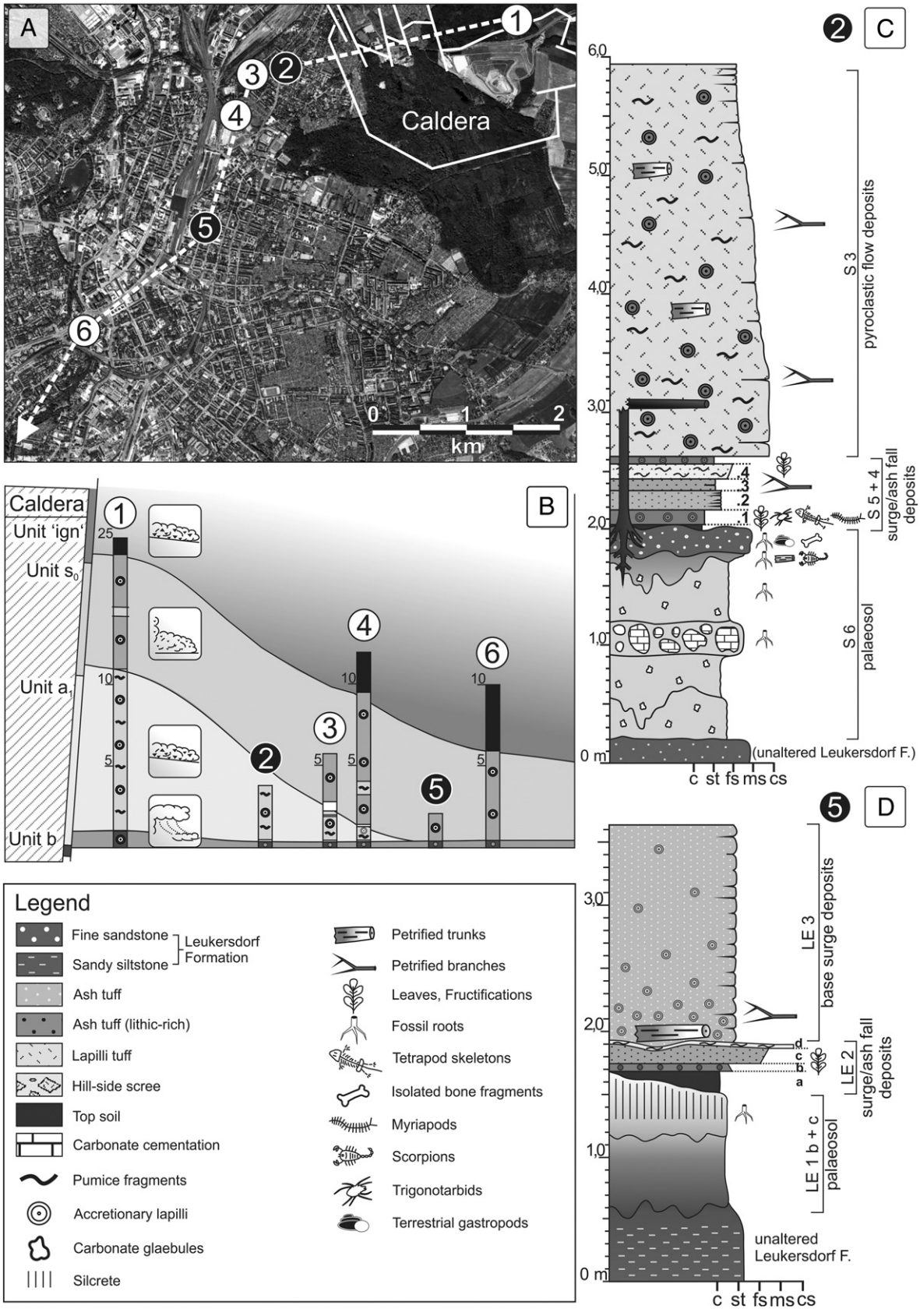

Fig. 3. Stratigraphic model of the Zeisigwald Tuff and excavation sections. (A) Estimated location of the Zeisigwald caldera in the NE of Chemnitz, as well as drillings and outcrops exposing the base of the Zeisigwald Tuff (1–6; 2—excavation site Hilbersdorf (C); 5—excavation site Sonnenberg (D)). (B) Distribution and architecture of the major pyroclastic units shown on a profile line diagrammed in '(A)': Unit b—surge and minor ash fall deposits; Unit a_1—pyroclastic flow deposit; Unit S_o—surge deposit; Unit ign—series of pyroclastic flow deposits (after Fischer, 1991). (C) Lithological section of the Hilbersdorf excavation. (D) Lithological section of the Sonnenberg excavation encompassing palaeosol (Unit LE 1) and the basal pyroclastics of the Zeisigwald Tuff (units LE 2 + 3), whereas Unit LE 2 correlates with Unit S 5 in the Hilbersdorf excavation.

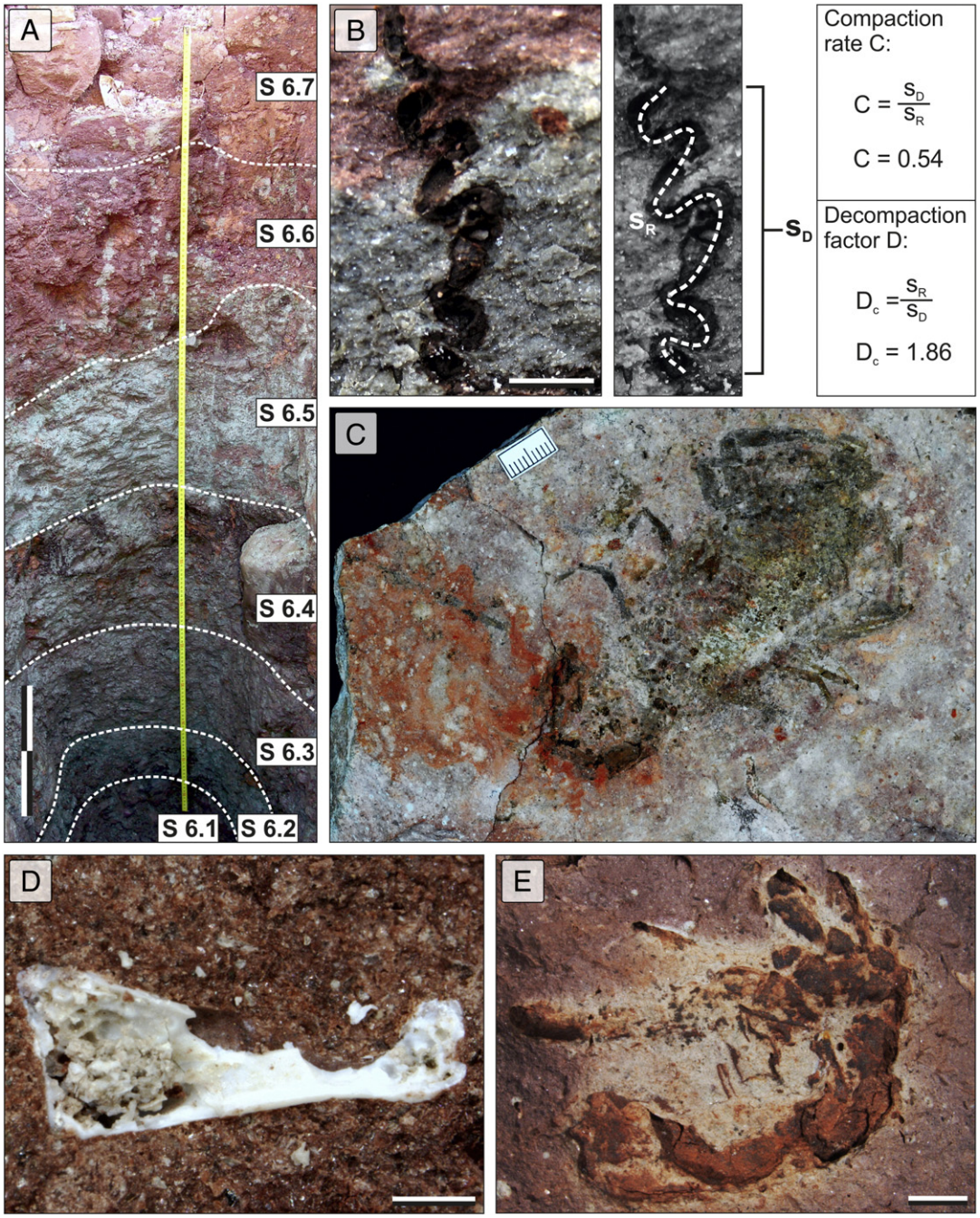

Fig. 4. Sedimentological and palaeontological record of the upper palaeosol units (S 6.6 + S 6.7) in the Hilbersdorf excavation. (A) Complete section of the palaeosol profile divided into sub-units showing a clear bisection between the lower bleached, carbonate-bearing phreatic part, and the upper red-coloured vadose part (scale bar: 0.40 m). (B) Vertical root showing convolution due to compaction. Compaction rate and decompaction factor were estimated by calculating the ratio between the length (s_R) and the distance from the upper and lower end (s_D) of the root (scale bar: 10 mm). (C) One of two completely and *in-situ* preserved scorpions found in their burrow a few centimetres below the palaeosol surface. The red coloured area marks the outline of the burrow and is caused by submerged clay minerals and iron oxides (polarised light, scale bar: 10 mm). (D) Bone fragment from unit S 6.7 preserved in fluorapatite ($Ca_5(PO_4)_3F$) with relicts of spongy tissue (scale bar: 0.5 mm). (E) Trigonotarbid arachnid preserved as partial ventral imprint on the palaeosol surface (scale bar: 2 mm).

surface, sparse and badly preserved plant remains can be found, although a typical litter horizon, which would usually consist of diverse organic components, is missing in the excavation site. These isolated remains were identified as shoots of large-leaved conifers and calamitaleans, as well as cordaitalean and pteridosperm leaf fragments and seeds (Rößler et al., 2012b). Slightly below the palaeosol surface larger pieces and horizontally oriented logs of silicified deadwood are preserved, which can be well distinguished from silicified roots. In one case, a calamitalean stem base of *Arthropitys bistriata* was rooting upon a cordaitalean deadwood trunk (Rößler et al., 2014). Besides these plant fossils, a variety of animal remains were found in the uppermost palaeosol. Frequently, small fossilised bone fragments being less than 10 mm and preserved as fluorapatite occur (Fig. 4D), but due to the small size it is often impossible to refer them to any specific vertebrate, with the exception of one amphibian clavicle and one reptile jaw with tiny teeth.

Another group of fossils, frequently occurring down to a depth of 0.4 m below the palaeosol surface, are 3–20 mm large terrestrial gastropods showing a trivial ornamentation (Fig. 5E). They belong to the genus *Dendropupa* (Rößler et al., 2012b) and seem to be related to

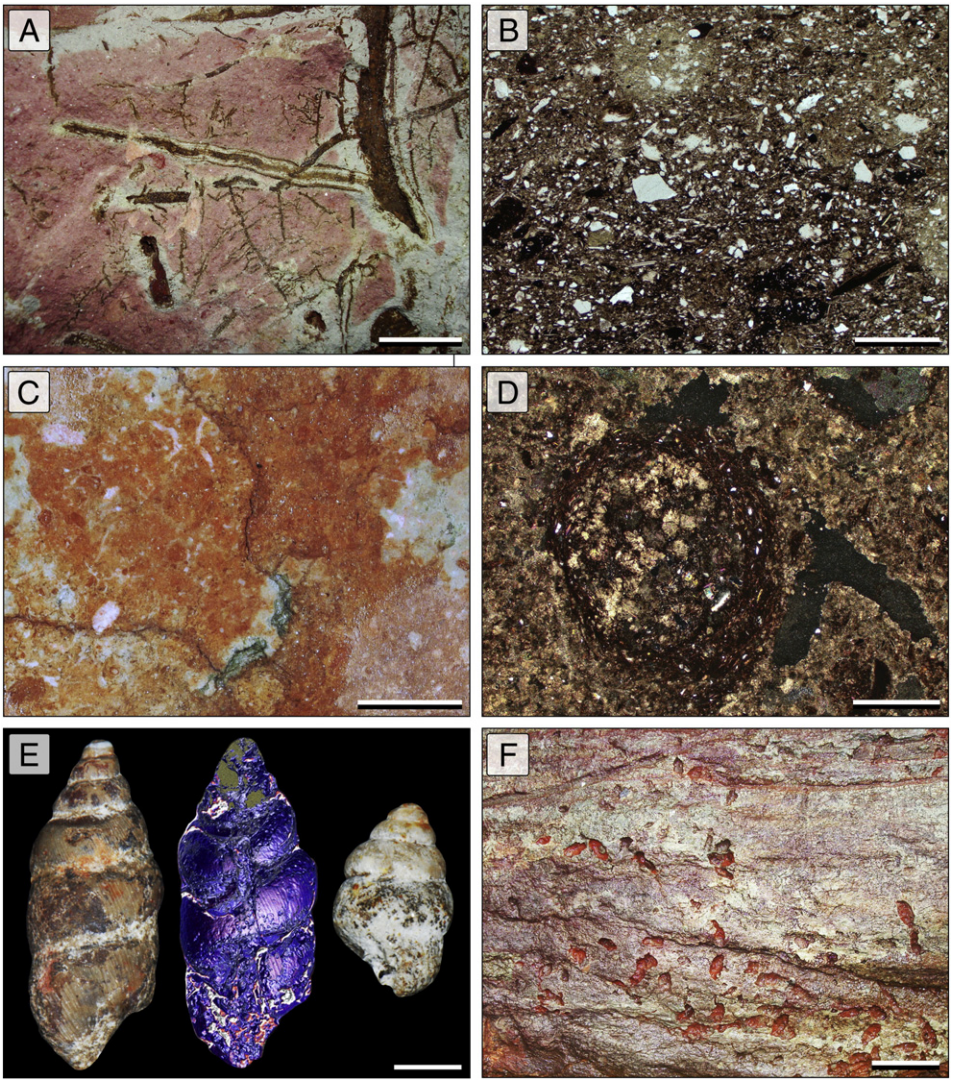

Fig. 5. Sedimentological and palaeontological record of the upper palaeosol units (S 6.6 + S 6.7) representing the vadose zone. (A) Horizontal surface of red-coloured, medium-grained sandstone of S 6.7, intensively pervaded by drab-haloed, flattened root traces filled with black-coloured manganese and iron oxides (scale bar: 20 mm). (B) Unaltered, poorly-sorted sediment of S 6.7, rich in angular quartz, feldspar grains and muscovite, surrounded by a silty matrix (plane-polarised light, scale bar: 1 mm). (C) Section of a carbonate glaebule from S 6.6 exhibiting colour mottling, tiny carbonate root tubes and iron oxide accumulation indicated by the red staining (scale bar: 10 mm). (D) Likely root tube in transverse section possessing a core filling by sparitic carbonate surrounded by a layered rim of haematite, alongside a branching carbonate root tube (thin section of glaebule in 'C', cross-polarised light, scale bar: 1 mm). (E) Silicified gastropods from S 6.7 exhibiting up to seven windings and trivial ornamentation (in the middle: Micro CT image of left specimen showing internal architecture; scale bar: 2 mm). (F) Mass occurrence of gastropods on a deadwood fragment, preserved as moulds filled with iron oxides (scale bar: 20 mm).

D. walchiarum Fischer from the lower Permian of France. Comparisons are also possible to *D. zareczenyi* Panow from the lower Permian of Poland (Stworzewicz et al., 2009) and *D. vestusta* from the lower Pennsylvanian of Nova Scotia, Canada (Falcon-Lang et al., 2004). The gastropods are preserved as moulds or casts, endocasts of manganese or iron oxides, and rarely as silicified shells. Because they are predominantly found in full-body preservation and mostly lack a sediment infill they are interpreted as being conveyed in their natural habit. They were frequently found occurring in the vicinity of roots and deadwood logs, sometimes forming discrete clusters. This observation leads to the consideration that the gastropods were ecologically linked in some way to the roots and deadwood pieces, probably feeding on microorganisms such as microarthropods, algae, fungi or bacteria and reveal an interesting type of interaction.

Besides a not yet identified trigonotarbid arachnid (Fig. 4E), the most spectacular finds made in the uppermost palaeosol are two complete scorpions and several associated ecdysis fragments, buried in their original burrows, a few centimetres below the palaeosol surface (Fig. 4C). These finds represent the first completely preserved scorpion body fossils from the Permian.

Units S 5 and S 4 are a 0.54–0.61 m thick succession of purple to light-grey/green-coloured, fine- to medium-grained, thinly bedded and unwelded ash tuffs. The pyroclastic deposits overlie the palaeosol with a sharp contact, which served as a sliding surface, induced by sub-recent gravitational slope gliding. Pyroclastics are subdivided into six horizons showing a coarsening-upwards, which is interpreted as a result of increasing eruption energy. Ash tuffs bear a high amount of lithic fragments originating from the bedrock, and an increasing fraction of flattened pumice fragments upward in the section. The series of thinly bedded pyroclastics is interpreted as a stacked deposit of low-concentrated flows, fine surges and accompanying ash falls, which originated from the initial eruption phase of the Zeisigwald volcano. The lowermost horizon S 5.0 represents a 0–0.05 m thick, very fine-grained and dark-purple-coloured fine-ash tuff, which is in wide parts badly preserved, due to sub-recent sliding processes. It contains single glass shards and seems to compensate the morphological relief of the

palaeosol surface. Frequently occurring fine roots indicate a small hiatus in the pyroclastic succession. This horizon is assumed to be the result of a minor ash fall occurring a certain time before the major eruption sequence started. Horizon S 5.1 is a poorly stratified, fine-grained, dark-purple-coloured ash tuff that bears accretionary lapilli up to 5 mm in diameter. It is interpreted as the initial fallout of a low-energy phreatomagmatic eruption that covered the former forest ground. The fossil record of this key horizon is particularly comprehensive and diverse in terms of preservation. Many fossils are buried *in-situ* and fossilised in great detail. There is a high abundance of plant adpressions of different size, as well as silicified branches and upright-standing plant axes. Although preservation of any organic matter is completely lacking, plant remains such as leafy twigs or fertile pinnae often exhibit organ connections (Rößler et al., 2009). Even adpression specimens in many cases reveal some kind of three-dimensional aspect (Feng et al., 2014). Moreover, articulated skeletons of reptiles and amphibians as well as adpressions or moulds of different kinds of arthropods (*Arthropleura*, diplopods), trigonotarbid and uropygid arachnids were found (Dunlop and Rößler, 2013; Rößler et al., 2012b). In contrast, fossils are rare in the overlying horizons, except for an upside-down embedded crown of a medullosan tree and some cordaitalean or pteridosperm leaf fragments in Unit S 4.

Unit S 3 is overlying Unit S 4 with an erosional contact and has a thickness of more than 3.35 m, which is limited due to recent weathering and erosion. This massive layer of light-red to purple-red colour is a poorly sorted, matrix-supported and unwelded lapilli tuff with large flattened pumice fragments (15–50 mm in diameter), abundant accretionary lapilli up to 12 mm in diameter, and minor amounts of lithic fragments. The unit is interpreted as an ignimbrite, deposited from a highly concentrated pyroclastic density current and correlating with the a_1 horizon *sensu* Eulenberger et al. (1995) of the Zeisigwald Tuff (Fig. 3B). In this unit, the small- to medium-sized upright-standing stems are toppled at a height of 1.5 m emphasising the destructive energy of this high-concentration pyroclastic flow. Other trunks lying horizontally in this layer were transported over small distances and orientated in an east–west direction. Further phenomena indicative of lateral transport are accretions of plant debris in the current shadow of trees. Bleaching haloes occurring around the petrified trunks and branches are the result of diagenetic processes that took place during the petrifaction of the wood. One of the most famous fossils found in this layer is the largest calamite documented in the world to date (*Arthropitys bistriata*) with an estimated length of 15 m (Feng et al., 2012; Rößler et al., 2012a). This outstanding fossil tree, showing multiple branching, a three-dimensional crown architecture, abundant secondary growth, challenged the conventional reconstruction of the calamitaleans. Unit S 3 is covered by sub-recent hill-side scree and a recent soil horizon.

2.4. The section at Sonnenberg excavation site

The second excavation was established in 2009, in Chemnitz–Sonnenberg (N 50°50′07.97″, E 12° 56′01.86″). It is situated c. 1.5 km S of the Hilbersdorf excavation site and 2 km SW of the estimated eruption centre (Fig. 3A). The 20 × 15 m large excavation area bears a similar potential to upgrade the fossil record of the Chemnitz Fossil Lagerstätte. The lithological profile encompasses the epiclastic palaeosol horizon and the overlying basal pyroclastics of the Zeisigwald Tuff (Fig. 3D). Due to compression tectonics, the beds show a general dip of c. 3° in WSW direction. The overall thickness of the section is about 3.10 m. It is subdivided into three units: the palaeosol at the base (Unit LE 1), overlain by basal, bedded ash tuffs (Unit LE 2) and a massive ash tuff (Unit LE 3).

The palaeosol developed upon alluvial deposits of the upper Leukersdorf Formation (LE 1a), which are represented by a red-coloured sandy siltstone. They show moderate sorting, a high amount of platy muscovite and angular quartz grains. The transition from the unaltered sediments to the palaeosol is gradational. In contrast to the unaltered red-coloured sediment of LE 1a, the up to 1 m thick palaeosol is characterised by the dark greyish to purple colour at the base (LE 1b) as well as light to the intense green colour at the top (LE 1c), whereas the transition from LE 1b to LE 1c shows typical colour mottling. A dominant feature of the palaeosol is the high clay content, especially in the lower 0.55 m thick LE 1b, which is therefore classified as Bt horizon. Slickensides occur frequently. The 0.35–0.50 m thick LE 1c, classified as A horizon, exhibits a massive fabric and is strongly lithified at the top, due to intense cementation by SiO_2; the high silica content, up to 90%, is most probably derived from the overlying pyroclastics by diagenetic migration. Root tubes occur not as frequently as in the palaeosol of the Hilbersdorf excavation site and are mainly preserved as adpressions, thinly coated by yellowish-brownish iron oxyhydroxide (goethite). Thickness variations of LE 1c seem to reflect the morphological relief of the palaeosol surface. Altogether, the palaeosol at the Sonnenberg excavation site represents a poorly drained substrate, which is likely to be formed under waterlogged conditions. Further investigations will elucidate the relation of palaeosol moisture regime and the floral assemblage.

The overlying basal, bedded pyroclastics of Unit LE 2 represent a c. 0.45 m thick succession of thinly-bedded, purple-coloured ash tuffs, which show a sharp contact with the underlying palaeosol and an inverse internal grading from the bottom to the top. These are subdivided into four horizons. LE 2a represents an intense dark purple-coloured, very fine-grained ash tuff possessing a thickness of 0–0.20 m. By accumulating upon the palaeosol the morphological relief is equalised. So far, a few plant debris relicts have been found. LE 2a is interpreted as the stratigraphic equivalent of Unit S 5.0 in the Hilbersdorf excavation site. LE 2b is a 0.05–0.06 m thick, dark-purple-coloured ash tuff with silt- to sand-sized components revealing a moderate sorting. Major components are vesicular glass shards, angular quartz crystals, lithic fragments, up to 1 mm large pumice fragments and up to 5 mm large accretionary lapilli. LE 2b bears silicified branches and leafy shoots of calamitaleans, cordaitaleans and psaroniaceous tree ferns, and can be correlated with the major fossil-bearing horizon S 5.1 at Hilbersdorf excavation site. The upper horizons LE 2c and 2d are characterised by an increasing grain size, an increasing amount of lithic fragments and up to 10 mm large pumice fragments. The latter appear concentrated in a 0.03 m thick layer at the top of LE 2d. Altogether, LE 2 is interpreted as a succession of low-concentrated pyroclastic surges and accompanying ash falls representing the stratigraphic equivalent of Unit S 5 at the Hilbersdorf excavation site. The slightly reduced thickness of LE 2 compared to S 5 may correspond to an increased distance to the eruption centre.

The uppermost Unit LE 3 is a light-purple- to red-coloured, massive ash tuff with a maximum thickness of 1.75 m at the excavation site, surely not representing the original thickness, which must have been much more, at the caldera border up to 50 m according to Eulenberger et al. (1995). Depositional features are a homogeneous grain size distribution of mainly coarse ash components and slightly visible bedding in the outcrop. Partly fragmented accretionary lapilli up to 10 mm in size occur frequently and are concentrated in the basal part. The matrix consists of vesicular glass shards, quartz crystals and minor lithic fragments. Besides highly fragmented remains of unidentified leafy shoots, a large petrified trunk with a diameter of 0.60 m was found in horizontal position on the top of LE 2, buried in LE 3 and orientated in NE–SW direction (Rößler and Merbitz, 2009). LE 3 is interpreted as the deposit of a low-concentrated pyroclastic flow with a major lateral component, comparable to a base surge, and pointing to a highly explosive, phreatomagmatic eruption. Whereas LE 3 seems to correlate with the S_o horizon of the Zeisigwald Tuff *sensu* Eulenberger et al. (1995), their a_1 horizon (= Unit S3 in Hilbersdorf) is lacking at Sonnenberg excavation site.

3. Material and methods

During the excavation in Chemnitz–Hilbersdorf the pyroclastic rock was removed bed by bed down to the palaeosol. Surfaces were

documented sector by sector, each 1 × 1 m in size encompassing sketches and descriptions in protocols and photographs. Measurement of the surface relief was done by tachymeter, producing three-dimensional data, from which a graphical computer model was developed (Rößler et al., 2012b). After recording the surface, the upper 0.40 m of the palaeosol was removed, fossils were collected and documented. The complete recovery of selected root systems related to upright-standing trees was a great challenge because of their three-dimensional habit and the often patchy preservation due to the state of silicification.

The complete palaeosol profile was exposed in two trenches, each having a depth of 2 m below the palaeosol surface with unaltered sedimentary rocks of the upper Leukersdorf Formation. Both palaeosol sections were investigated in great detail, comprising profile descriptions, sampling for thin sections and geochemical analyses. In addition, twelve further rock samples were collected from the uppermost palaeosol subhorizon (S 6.7) for geochemistry to ensure representative results for the whole excavation area. Samples were chosen by following the systematic grid of squared sectors, used for spatial documentation. Whole rock geochemical analyses of major and trace elements were carried out at the Geological and Palaeontological Institute of the Charles University Prague by using ICP-OES and titration for determination of Fe^{2+}/Fe^{3+}. Furthermore, qualitative mineral analysis of whole rock powder fraction was done by X-Ray diffraction.

Results of sedimentological and geochemical investigations are supplemented by palaeobotanical data. Root systems of the upright-standing trees were excavated and, as fully as possible, reconstructed and the best preserved specimens of all plant groups were chosen (19 of 53). The root systems were graphically reconstructed on the basis of observations listed in the protocols during recovery.

Preliminary results of wood anatomical studies are presented, which also show the potential for gaining additional environmental data. Several specimens of woody arboreal plants, calamitaleans in particular, show distinct tissue density variations in their secondary xylem, which probably reflect growth ring-like patterns. They were investigated in planar sections of the specimens K3257 (*Arthropitys sterzelii*, see Rößler and Noll, 2010), KH0277 and KH0052 (*Arthropitys bistriata*) and K5200 (*Arthropitys ezonata*, see Rößler and Noll, 2006). Criteria for qualitative evaluation of tissue density variations are cell size, cell wall thickenings, destructive patterns of cell lumen, presence of callus tissue as well as circumferential continuity in the stem.

In order to investigate the internal anatomy of the petrified trees, we used a sand blaster to clear the stem's surfaces. Specimens were subsequently cut with a trimming saw to reveal transverse sections. The latter were ground and polished according to standard procedures (e.g., Taylor et al., 2009) and examined using reflected light microscopy. Sections were photographed under reflected light using a Nikon DS-5 M-L1 digital camera attached to a Nikon SMZ 1500 microscope. Overview photographs were made by using an Epson Perfection V330 scanner. The specimens are stored at the Museum für Naturkunde Chemnitz.

4. Results

The fossil forest ecosystem developed on a mineral substrate in an alluvial plain environment. However, the greater detail described herein for the Hilbersdorf excavation site depicts just a small window that gives insight into a very local habitat of the whole forested area.

4.1. Significance of the palaeosol profile

We focus here on diagnostic macroscopic features, which are often recognisable in the field (Mack et al., 1993; Retallack, 1988), and on geochemical proxies (see Section 4.2). The soil cover provides key information about the environment. This is important for interregional comparisons, which reveal how they change across continents. Comparable to modern soils, the soils of the past provide a highly appropriate proof of the land surface environment back to deep time. Palaeosols link local climatic conditions and geomorphology with parent material and time as the main controlling influences. Because of the additional information they yield on the biosphere and the vegetation cover in particular, they play a crucial role as natural archives recording environmental changes over geological spans of time (Birkeland, 1999; Retallack, 2001). Nevertheless, burial and diagenesis can modify palaeosols, change their chemical properties and complicate distinguishing between the results of pedogenetic and diagenetic processes (Wright, 1992). Although research on palaeosols has developed as a major topic in geologically younger strata (Achyuthan et al., 2012; Kraus and Hasiotis, 2006; Lu et al., 2015; Vacca et al., 2012; Wagner et al., 2012) there are also examples to solve both stratigraphic and palaeoecological questions in the Palaeozoic (Besly and Fielding, 1989; Mack et al., 2010; Rosenau et al., 2013; Tabor and Poulsen, 2008; Tabor et al., 2011).

4.1.1. Pedogenic features and composition of the palaeosol

The standing vegetation was found rooting in a clastic alluvial palaeosol. The dominating red colour of the sediments indicates that they were deposited on a predominantly well-drained alluvial plain. Green bleaching around different-sized organic matter, such as roots, leaf fragments or seeds/ovules is frequently present and the typical mottling as well (Figs. 4A and 7). The grain size ranges between silt and medium sand with a minor percentage of clay fraction. In the uppermost part, medium-sized, semi-rounded quartz pebbles occur sporadically. Due to bioturbation by plants and soil organisms the original stratification of the former substrate is nearly completely overprinted, but in exceptional cases still preserved. The uppermost 0.30 m of the palaeosol is lithified and bears a high potential for fossil preservation (Figs. 4 and 5). On the basis of colour and compositional variations, the palaeosol profile was subdivided into seven horizons from S 6.1–S 6.7, bearing information on different stages of soil formation (Fig. 7). All horizons show a diffuse gradual transition at base and top and vary laterally in thickness, except for S 6.4. Furthermore, horizons show a more or less consistent grain-size distribution with a slight coarsening-up tendency. The same holds true for the original mineral composition of the sediment, which mainly consists of quartz, muscovite, metamorphic rock fragments originating from the Variscan basement in the source area and feldspars such as plagioclase and orthoclase (Fig. 5B). Mineral grains are poorly sorted and generally angular to sub-angular indicating a low maturity of the original sediment. The same trait is shown in the lowermost horizon S 6.1 that represents the unaltered, original alluvial sediment, typical for the upper Leukersdorf Formation (Schneider et al., 2012). The red silty sandstone of S 6.1 shows small patchy areas of green colour and contains a low amount of carbonate. Besides quartz, metamorphic rock fragments and feldspars (orthoclase, plagioclase), the composition of the sediment is characterised by a high amount of muscovite (up to 20%). Haematite and clay minerals are present as minor components. Carbonate occurs in small elliptical areas, where it replaced the original matrix material. The sorting of the matrix-supported sediment is poor, mineral grains are angular to sub-angular. In outcrop, S 6.1 seems to be massive, no bedding structures were recognised. No clear evidence for intense chemical weathering was found at either the macroscopic or microscopic scale.

The transition to the overlying palaeosol (horizons S 6.2–6.7) is diffuse. Except for the uppermost horizon S 6.7, an extended portion of the profile underwent sub-recent weathering, resulting in considerable delithification. S 6.2–S 6.6 exhibit a more or less clear bisection into a lower greenish-coloured or mottled part, and an upper red-coloured part. The colour transition is confluent and strongly fluctuates with depth, which is well illustrated in the profile shown in Fig. 4A. In the profile, the red-coloured part (S 6.6 and S 6.7) reaches a depth of 0.50 m below the palaeosol surface, whereas in other areas of the

excavation the bleached part (S 6.2–S 6.5) reaches up to the palaeosol surface, so that residually red-coloured areas remain restricted to the uppermost 0.20 m.

Horizons S 6.2–S 6.5 consist of silty to fine-sandy sediment, commonly with carbonate glaebules of 5–100 mm in size, and finely distributed carbonate cement occurring in residual decimetre-sized hard lenses and blocks. No original bedding structures are present; they are destroyed by pedogenic processes and carbonate formation, respectively. S 6.3 shows an intense colour-mottling between green and purple, indicating fluctuating Eh conditions (Fig. 7). Additionally, clay minerals show a woven bright clay microfabric (omnisepic), which points to a repeated swelling and shrinkage (Brewer, 1976). Upwards in the profile, S 6.4 bears large, decimetre-sized carbonate blocks that aggregate a dense, nearly impervious layer of 0.30–0.40 m thickness throughout the whole excavation site (Fig. 6A, B). Smaller carbonate glaebules occur in close association below and above the carbonate horizon. Some of them reveal a relict red-coloured core, coated by a greenish rim. EDX analyses on single carbonate crystals and whole-rock-geochemistry revealed a low Ca/Mg-ratio leading to a classification as High-Mg-Calcite. XRD analyses detected dolomite as a major component of S 6.3 and S 6.4. The presence of dolomite was also proven in thin sections made of glaebules, blocks and lenses (Fig. 6D). Altogether, four different types of carbonate cement have been recognised. The matrix in all samples mainly consists of equigranular, microsparitic cement that shows a dense fabric of fine crystallinity (20–100 μm). Grain boundaries are irregular, possibly due to diagenetic leaching (Fig. 6D). This type frequently changes into coarser, inequigranular microsparitic cement with subhedral crystal boundaries and occasional euhedral rhomboid dolomite crystals. Besides the aforementioned matrix cements, macrosparitic drusy cements and megacements occur as infill of fissures, vugs, small cavities, and also tiny root tubes (Fig. 6D, E). Frequently, cavities are filled with single crystals. Where carbonate cementation appeared, the components of the original clastic sediment are almost completely replaced, which is indicated by leached quartz grains floating in the carbonate matrix, altered mica sheets adjusted parallel to the margins of the recrystallisation fronts, and a major depletion of SiO_2 and Al_2O_3. Slightly above the massive carbonate of S 6.4 so-called 'displacive structures' *sensu* Watts (1978) were recognised (Fig. 6F).

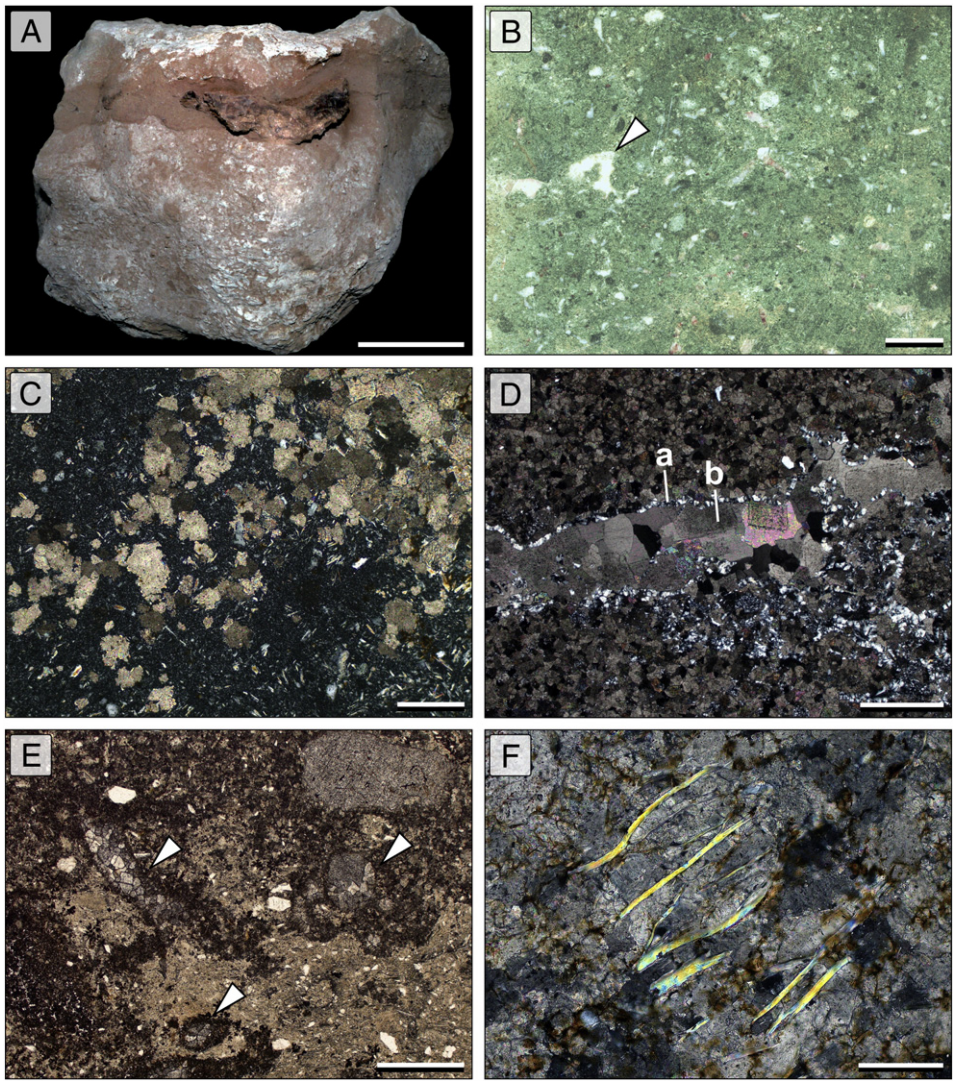

Fig. 6. Sedimentological and mineralogical features of the lower palaeosol sub-units (S 6.3–S 6.5) representing the phreatic zone. (A) Carbonate block of S 6.4 as part of the groundwater calcrete showing a weathered surface and a layer of authigenic silica and a dark chert lense within (scale bar: 0.1 m). (B) Section of a carbonate block (S 6.4) of greenish coloured massive carbonate and bright coloured root tubes filled with sparitic cement (arrow, scale bar: 10 mm). (C) Brownish carbonate cement with dissolved crystal grain boundaries due to replacement by local accumulation of silica in a carbonate glaebule (S 6.3, cross-polarised light, scale bar: 0.2 mm). (D) Multiple-phased crystallisation of marginal chalcedony (a) and central coarse-grained idiotopic dolomite (b) in a void, surrounded by a matrix of equigranular, microsparitic cement (S 6.4, cross-polarised light, scale bar: 1 mm). (E) Tiny root tubes in longitudinal and transverse view filled with sparitic cement (arrows) in a carbonate glaebule of S 6.5 (plane-polarised light, scale bar: 1 mm). (F) 'Displacive structure' *sensu* Watts (1978) showing single muscovite plates, which were drifted apart during rapid carbonate formation (S 6.5, cross-polarised light, scale bar: 0.1 mm).

Several of the carbonate blocks contain irregularly shaped, centimetre-sized lenses of black chert consisting of cryptocrystalline silica (Fig. 6A). In the vicinity of these lenses, silica is also present as marginal infill of small cavities, forming multiple layers of chalcedony (Fig. 6D). The centre of the cavities is often filled with macrosparitic carbonate cement, mainly dolomite. Cryptocrystalline silica cementation was also recognised in thin sections of carbonate glaebules from the over- and underlying horizons. Silica often surrounds or borders leached carbonate crystals and contains high amounts of the original clastic sediment, e.g., feldspar or muscovite (Fig. 6C).

Relicts of biogenic components are rare in the lower horizons, with the exception of tiny root tubes frequently occurring in S 6.4 and S 6.5, but never beneath (Fig. 6B, E). They are up to 2 mm in diameter, sometimes show furcation and are always filled with macrosparitic cement.

Horizons S 6.6 and S 6.7, representing the upper part of the palaeosol profile, exhibit a variable thickness of 0.40–0.50 m. The top of S 6.7, the palaeosol surface, shows a sharp contact to the overlying basal pyroclastics. The original reddish-brown colour is interspersed with light-green bleaching dots. In comparison to the unaltered sediment (compare S 6.1), S 6.7 shows only minor compositional differences. The sediment is dominated by angular to sub-angular quartz and muscovite (Fig. 5B). Lithic fragments and feldspar occur as minor components. Unusually, mineral grains do not or rarely show chemical alteration. The fabric is massive and supported by a clayey and silty matrix, rich in haematite. Millimetre- to centimetre-sized ferritic concretions occur frequently, especially in S 6.6. In this horizon they appear together with carbonate precipitates, whereupon a core of carbonate is covered with concentric rims of haematite, which is regarded as an *in-situ* formation (Fig. 5C–D). Dislocation of clay minerals from the upper horizon down to lower horizons was observed, but is most probably due to modern weathering processes (Retallack, 1988).

At the top of the palaeosol, S 6.7 and S 6.6 supported dense vegetation dominated by hygrophilous elements and is completely pervaded by different kinds and sizes of roots (Fig. 5A). These roots exhibit different states of preservation, such as silicified organs showing cellular preservation up to root tubes or haloes. The majority of roots remained as flattened moulds with an infill of black-coloured manganese/iron oxides and bleaching haloes around them. The roots are predominantly positioned horizontally in the uppermost part of the palaeosol horizon (S 6.7) and rarely show furcation patterns. In contrast, deeper in the profile (0.20–0.35 m, S 6.6), roots occur as finely distributed moulds forming a dense network, which seems to be partly decomposed. This type of root was not observed in the whole excavation site, but in wide parts and has no relation to single specimens of the upright-standing plants. The root systems of the latter occasionally remained in an incomplete silicified state, reaching down to a maximum depth of 0.70 m (Fig. 9F), but in average not deeper than 0.40 m.

Millimetre-sized bone fragments, frequently occurring in S 6.7 (Fig. 4D), are preserved as fluorapatite ($Ca_5(PO_4)_3F$) as proved by XRD analysis (Rößler et al., 2010). With regard to diagenetic processes, it is important to mention that they still exhibit both their original shape and calcium portion.

4.1.2. Interpretation

As illustrated by Schneider et al. (2012), the Hilbersdorf excavation site is situated in a basinal position of the north-eastern part of the Chemnitz Basin. The depositional environment is interpreted as a distal alluvial braidplain. The common sediment type is that as characterised for horizon S 6.1, mainly representing fine-grained overbank and sheet flood deposits. These have a low maturity, indicating a short transportation distance from the source area represented by the surrounding Variscan metamorphic units. The same parent material can be assumed for the overlying palaeosol succession (S 6.2–6.7), which underwent pedogenetic processes and reflects them to various degrees. With regard to surface-weathering processes, the palaeosol profile can be subdivided into a phreatic (S 6.2–6.5) and a vadose zone (S 6.6 and 6.7).

The occurrence of a carbonate horizon in S 6.4, bearing large carbonate blocks accompanied with intense bleaching in the phreatic zone, is one of the most striking features of the palaeosol. The large carbonate blocks are seen as residuals of a former massive calcrete horizon, which was leached in parts by sub-recent weathering, because the blocks exhibit a weathered surface (Fig. 6A) and are surrounded by dark-grey mud, rich in manganese oxides. As will be substantiated subsequently, we interpret this level as a groundwater calcrete. Carbonate formation is a common feature in ancient and recent soils in regions of semi-arid to sub-humid climate (e.g., Alonso-Zarza, 2003; Khadkikar et al., 1998; Mack et al., 2000; Pimentel et al., 1996; Retallack, 2001; Thiry and Milnes, 1991; Wright, 2007). Carbonate formation could be either caused primarily, by ascending pore water in the vadose zone of the soil profile (Gile et al., 1966; Klappa, 1980; Machette, 1985; Schneider and Rößler, 1995; Watts, 1980), or secondarily, by carbonate precipitation from a highly saturated groundwater (Alonso-Zarza et al., 2011; Arakel, 1986; Nash et al., 2004; Semeniuk and Meagher, 1981; Spötl and Wright, 1992). Based on specific traits for the distinction of pedogenic and groundwater calcretes (Pimentel et al., 1996), the groundwater interpretation of S 6.4 is most likely for the following reasons. It shows (1) a gradational transition to the under- and overlying sub-horizons in association with colour mottling and bleaching caused by iron translocation in a reducing environment, (2) a massive fabric in the carbonate blocks, a typical alpha-fabric in microscopic scale *sensu* Wright (2007), and (3) a wide range of different crystal sizes with tendency to coarse-grained cementation. In addition, the low Ca/Mg-ratio and a high abundance of dolomite support this interpretation. Moreover, the formation of authigenic silica in the carbonate blocks of S 6.4 is a typical process, commonly observed in groundwater calcretes (Alonso-Zarza et al., 2011; Nash and Ullyott, 2007). It is likely to be seen as a result of replacement of the original clastic sediment, when silica was discharged by dissolution of quartz and silicates. Dissolved silica then accumulated in vugs or cavities and led to local replacement of the carbonate cement (Fig. 6C). The infill of small cavities with multiple layers of chalcedony at the margins reveals that replacement, dissolution and accumulation of silica during carbonate formation was a multi-staged process, which was later presumably overprinted by diagenesis. In general, diagenetic processes have to be taken into account regarding the overprint of the original carbonate fabric, as it is proven by evidence for recrystallisation, neomorphism and dolomitisation. Carbonate precipitation at the top of the groundwater table was a fast elapsing process, supported by an initially highly saturated fluid. This is indicated by displacive structures in carbonate glaebules in S 6.5 (Fig. 6F), slightly above the massive calcrete (Watts, 1978). Carbonate formation was probably initiated by a high evapotranspiration rate under dry conditions. Normally, formation of soil carbonate occurs in arid to semi-arid climates, infrequently under sub-humid conditions but also in wetland environments (Alonso-Zarza, 2003; Alonso-Zarza et al., 2011). Mack and James (1994) quote to a maximum MAP of 1000 mm/a, under which calcrete formation is possible. Intense colour mottling resulting from alternating Eh conditions, accompanied by microscopic swell-and-shrink structures of oriented clay minerals, gives evidence for a fluctuating groundwater table, which could be seasonally driven (Brewer, 1976; PiPujol and Buurman, 1994; Retallack, 2001). The frequent occurrence of tiny root tubes in the calcrete is a phenomenon that is commonly observed in pedogenic calcretes (Pimentel et al., 1996), but does not really contradict the interpretation as a groundwater calcrete (Fig. 6B). Probably, in the studied profile an initial pedogenic calcrete was succeeded by a groundwater calcrete. Typical fibrous cements and laminar marginal accretion of carbonate are absent. Rhizoliths in groundwater calcretes are described in connection to phreatophytic plants, which develop deep roots down to the groundwater level as a survival strategy to resist

longer periods of drought (Canham et al., 2012; Purvis and Wright, 1991; Semeniuk and Meagher, 1981). Here, it is assumed that the rhizoliths are relicts of a low vegetation cover during an earlier soil forming phase, which probably has been preserved by a primary pedogenic carbonate formation, later overprinted by the influence of groundwater leading to formation of the massive calcrete. The depth of a calcrete horizon correlates well with mean annual precipitation, which was proven by numerous data sets from modern and ancient soils (e.g., Jenny, 1941; Retallack, 1994, 2005). By infiltrating the palaeosol, low-pH rain water causes dissolution of near-surface soil carbonate and leads to translocation to deeper soil horizons. The depth of the calcrete horizon at Hilbersdorf excavation site is 0.80 m, reflecting the equilibrium level between surface water and groundwater. As compaction of the palaeosol during burial has to be taken into account (Caudill et al., 1997), it is necessary to ascertain the decompacted thickness of the palaeosol section, which overlies the calcrete horizon (S 6.4). Due to the fact that data concerning burial depth are lacking, the compaction rate was estimated by "re-stretching" a contorted, vertically downward-oriented root, according to the method applied by Caudill et al. (1997) for clastic dikes. The resulting compaction ratio of C = 0.54 would yield a depth to the calcrete horizon of ca. 1.50 m (Fig. 6B). Considering that a root is not propagating exactly vertically the real original depth to calcrete horizon was probably slightly less. Palaeoprecipitation was estimated by using the equation of Retallack (2005) for mean annual precipitation, where D is the depth to carbonate horizon:

$$P = 137.24 + 6.45D + 0.013D^2 \quad (1)$$
$$R^2 = 0.52;\ Standard\ error: \pm 147\ mm$$

As a result, a mean annual precipitation of P = 812 ± 147 mm/a was calculated.

In contrast to the phreatic zone represented by S 6.2 to S 6.5, the upper part of the palaeosol profile was not influenced by secondary diagenetic overprint and still shows primary pedogenic features, which can be used for reconstructing palaeoweathering conditions. This upper section (S 6.6 and S 6.7) shows a low maturity and can be classified as an Entisol, according to Retallack (2001). Nevertheless, classification systems of recent soils are complex and never-endingly controversial, and their application to palaeosols is challenging since the duration and amount of moisture in the soil, being major traits in recent soil taxonomy, cannot be substantiated (Mack et al., 1993; Retallack, 2001). Grain-size distribution suggests good aeration and drainage properties under moderate pH values, indicated by the red sediment colour in combination with dark-coloured root moulds, surrounded by green, bleached haloes (Kraus and Hasiotis, 2006). The haematite-rich matrix and small ferritic glaebules indicate chemical weathering under warm and humid conditions (PiPujol and Buurman, 1994; Widdowson, 2007). However, this is not confirmed by the nearly unaltered state of quartz and feldspar grains that likely reflects the low maturity of the substrate. Regarding this, a relatively short exposition time can be assumed. The co-occurrence and intergrowth of glaebules consisting of both carbonate and haematite (Fig. 5D) is a clear indicator for distinct climatic seasonality, caused by alternation of dry and wet phases (PiPujol and Buurman, 1997; Retallack, 1994; Sehgal and Stoops, 1972). Carbonate precipitates during dry phases with high evaporation rates, whereas haematite formed during phases of increased humidity (Retallack, 1994). Glaebules that show alternating rims of carbonate and haematite were reported from soils subjected to periodic changes in moisture availability that may also cause groundwater-table fluctuations (Sehgal and Stoops, 1972). The set of features revealed by the palaeosol at Hilbersdorf excavation site points therefore to soil-forming processes under seasonal climatic conditions. In monsoonal tropical soils, there are differences in root activity between wet and dry seasons (Singh and Singh, 1981), which cause temporal variations in respiration patterns. Carbonate precipitated at shallow depths during the dry season is partly dissolved by respiration of fine shallow roots, then further dissolved by respiration of deeper roots later in the wet season, as indicated by dissolution rinds and interlaminated goethite in carbonate glaebules of monsoonal soils (Courty and Fédoroff, 1985; Sehgal and Stoops, 1972) and palaeosols (Retallack, 1991). Because soil profiles continuously adjust in response to environmental influences, such as sediment supply, changes in local relief, temperature, rainfall, evaporation and vegetation cover, often results in some kind of polygenetic palaeosol, more or less reflecting successive stages of palaeosol formation. Although soil fabrics usually remain unaltered, it seems difficult to infer the palaeoclimate only from a single palaeosol sequence as investigated at our Hilbersdorf excavation site. Here we try to link micromorphological and compositional pedogenic characteristics with other indications of the habitat, such as geochemical proxies or anatomical structures of woody plants that colonised the parent substrate.

4.2. Geochemical proxies and traits of early diagenesis

Results of geochemical analyses comprise information on major element variations in the vertical section of the palaeosol profile and on horizontal variations in the excavation area referred to the uppermost Horizon S 6.7 (Table 1). Major element data are presented as weight percentages. Measurements of the whole fraction embrace the portion of annealing loss. Weight percentages of major elements were recalculated by extracting the amount of annealing loss. Weight percentages were then converted into moles, marked by simple element notation (e.g., Al instead of Al_2O_3), as suggested by Sheldon and Tabor (2009).

4.2.1. Major and trace element distribution in the vertical section

To evaluate sedimentological and pedogenic processes, different major and trace element ratios were plotted in the vertical section of the palaeosol profile (Fig. 7). The Ti/Al ratio represents a reliable indicator for provenance (Sheldon and Tabor, 2009). As expected, it shows just minor changes in the vertical section and refers to a consistent source area. By reflecting the clay content (Ruxton, 1968), the Al/Si ratio shows no major differences between the palaeosol horizons. This is of particular interest for the upper horizons S 6.5–S 6.7 because the constant ratio confirms the field observation that formation of a clayey Bt horizon by lessivage seems to be absent. Major element distribution in the vertical section is generally strongly dependent on carbonate formation. The carbonate-bearing horizons S 6.2–S 6.5, but in particular the calcrete horizon S 6.4, show an enrichment in Mg, Ca and Mn, whereas especially Si, Al, K and Fe (total) are depleted (Table 1). This is also expressed in the ∑ bases/Al (Ca + Mg + Na + K/Al) ratio, which is an indicator for weathering processes like hydrolysis (e.g., Retallack, 2001). Due to the presence of carbonate, the palaeosol is base-rich (Sheldon et al., 2002). Changes of Eh in the vertical section are shown by the Fe (total) + Mn/Al ratio (Retallack, 2001). Surprisingly, values do not reflect any difference between the vadose zone of the red-coloured horizons S 6.6 and S 6.7, which was under aerobic conditions and the bleached phreatic zone (S 6.2–S 6.5). However, the high Fe (total) + Mn/Al ratio of S 6.6 compared to the lower ratio of S 6.7 confirms the field observation of an accumulation of haematitic glaebules in S 6.6. The U/Th ratio is another proxy reflecting leaching processes or Eh conditions, respectively (Sheldon and Tabor, 2009). It shows a strong dependency to carbonate formation, which is mainly a result of thorium depletion in the carbonate-bearing horizons. By comparing values of all element ratios from the upper horizons S 6.6 and S 6.7 with the unaltered sediment (S 6.1) it is conspicuous that particularly values of Al/Si, Fe + Mn/Al and ∑ bases/Al are very similar. This supports the conclusion of a very immature palaeosol that has not experienced intense chemical weathering.

Table 1
Geochemical data of major and trace elements of the palaeosol presented in molar fraction (annealing loss included).

Horizon	Selection	Si	Ti	Al	Fe^{3+}	Fe^{2+}	Mn	Mg	Ca	Na	K	U	Th
S 6.1	Vertical profile	1.1500	0.0076	0.1499	0.0363	0.0059	0.0007	0.0521	0.0117	0.0130	0.0531	0.0157	0.,0629
S 6.2	Vertical profile	1.1841	0.0033	0.1166	0.0186	0.0051	0.0018	0.0595	0.0865	0.0025	0.0464	0.0105	0.0607
S 6.3	Vertical profile	1.2424	0.0041	0.0892	0.0134	0.0025	0.0031	0.1150	0.1028	0.0056	0.0273	0.0063	0.0211
S 6.4	Vertical profile	0.6077	0.0037	0.0821	0.0130	0.0014	0.0170	0.4719	0.5335	0.0050	0.0244	0.0114	0.0159
S 6.5	Vertical profile	0.9571	0.0059	0.1294	0.0122	0.0034	0.0052	0.0724	0.3142	0.0085	0.0475	0.0185	0.0380
S 6.6	Vertical profile	1.1498	0.0068	0.1395	0.0518	0.0063	0.0007	0.0425	0.0128	0.0080	0.0444	0.0237	0.0426
S 6.7	Vertical profile	1.1474	0.0058	0.1459	0.0315	0.0049	0.0007	0.0352	0.0317	0.0086	0.0581	0.0195	0.0489
S 6.7	Area	1.1308	0.0071	0.1571	0.0294	0.0063	0.0009	0.0303	0.0210	0.0100	0.0683	–	–
S 6.7	Area	1.0910	0.0075	0.1450	0.0336	0.0046	0.0005	0.0185	0.0483	0.0078	0.0787	–	–
S 6.7	Area	1.1400	0.0069	0.1490	0.0387	0.0048	0.0015	0.0269	0.0181	0.0098	0.0629	–	–
S 6.7	Area	1.2221	0.0069	0.1321	0.0081	0.0053	0.0005	0.0210	0.0299	0.0125	0.0683	–	–
S 6.7	Area	1.1315	0.0051	0.1261	0.0309	0.0041	0.0007	0.0227	0.0632	0.0067	0.0594	–	–
S 6.7	Area	1.1943	0.0064	0.1384	0.0249	0.0061	0.0007	0.0279	0.0184	0.0092	0.0611	–	–
S 6.7	Area	1.1797	0.0075	0.1498	0.0271	0.0093	0.0010	0.0325	0.0094	0.0107	0.0584	–	–
S 6.7	Area	1.1412	0.0073	0.1532	0.0295	0.0066	0.0009	0.0375	0.0205	0.0097	0.0643	–	–
S 6.7	Area	1.1078	0.0058	0.1397	0.0272	0.0070	0.0005	0.0263	0.0616	0.0071	0.0668	–	–
S 6.7	Area	1.0976	0.0070	0.1516	0.0336	0.0079	0.0014	0.0340	0.0393	0.0092	0.0663	–	–
S 6.7	Area	1.1521	0.0085	0.1485	0.0221	0.0060	0.0014	0.0304	0.0329	0.0100	0.0633	–	–
S 6.7	Area	1.2113	0.0061	0.1342	0.0191	0.0055	0.0009	0.0237	0.0148	0.0091	0.0701	–	–

4.2.2. Palaeoweathering indices

Quantification of chemical weathering in clastic sediments has proven to be a powerful tool for palaeoenvironmental studies in the last decades (Nesbitt and Young, 1982; Sheldon and Tabor, 2009; Sheldon et al., 2002). Here, we use a variety of approved methods, e.g., based on CIA, CIW or CALMAG, which contribute to our understanding of ancient weathering conditions under which the Chemnitz Fossil Forest developed. Methods were applied on the upper palaeosol horizons S 6.6 and S 6.7, which are in contrast to the lower horizons S 6.2–S.6.5, part of the vadose zone and thus solely influenced by surface weathering processes. For quantification of chemical weathering processes the following equations were applied:

$$\text{Nesbitt \& Young (1982)}: \quad \text{CIA} = 100 \times \frac{\text{Al}}{\text{Al} + \text{Ca}* + \text{K} + \text{Na}} \tag{2}$$

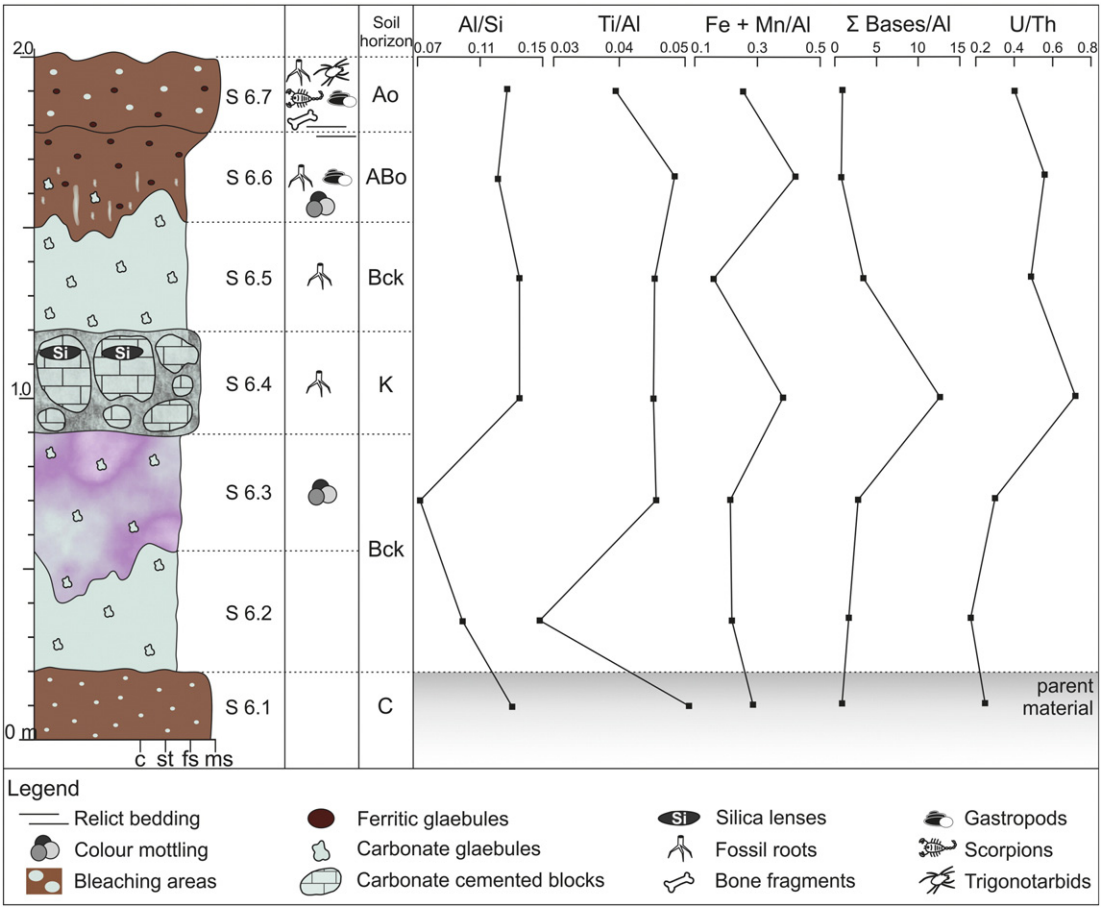

Fig. 7. Pedogenic characteristics and selection of major element ratios of the palaeosol at Hilbersdorf excavation site. Colours in the profile sketch are close to original colours documented in the outcrop. Classification of soil horizons is based on classification scheme proposed by Retallack (2001). Geochemical proxies show the comparison to the unaltered parent material represented by S 6.1 (C horizon).

$$\text{Harnois (1988)}: \quad \text{CIW(CIA-K)} = 100 \times \frac{\text{Al}}{\text{Al} + \text{Ca} * + \text{Na}} \tag{3}$$

$$\text{Nordt \& Driese (2010)}: \quad \text{CALMAG} = 100\text{x} \frac{\text{Al}}{\text{Al} + \text{Ca} + \text{Mg}} \tag{4}$$

Original CIA values can be influenced by sediment grain-size variations, a higher amount of CaO originating from carbonate, and mobility of K^+ especially during diagenesis (Fedo et al., 1995; Shao and Yang, 2012). For the analysed samples grain-size variations can be excluded because grain size is more or less stable in all samples. Occurrence of carbonate, however, seems to be likely. This is indicated by a higher amount of CaO compared to Na_2O. The original portion of CaO is determined by applying the method of McLennan (1993). The recalculated portion of calcium is quoted as Ca* or CaO*, respectively. The influence of potassium mobility can be validated by using the chemical index of weathering (CIW or CIA-K), which was proposed by Harnois (1988). However, Fedo et al. (1995) discourage the use of CIW because it does not involve the accompanying loss of aluminium. Most likely, comparison of both the CIA and the CIW will provide the best evidence for ancient weathering processes. In contrast to CIA and CIW, the CALMAG equation includes magnesium and calcium portions derived from carbonate weathering, which are the most reliable indicators of annual palaeoprecipitation (Nordt and Driese, 2010). However, the CALMAG was developed for vertisols, and therefore its applicability for the investigated palaeosol has to be documented.

The thirteen analysed samples of S 6.7 and S 6.6 show CIA values in a range of 54 to 57 (Fig. 8A). According to Nesbitt and Young (1982), CIA values commonly range from 50 to 70, whereupon unaltered feldspar has a value of 50 and unaltered sediment values between 60 and 70. In contrast, intensely weathered soils of the tropics exhibit CIA values of around 100. In addition to the macro-morphological features, the low CIA values of the analysed palaeosol samples are another indicator for a low chemical weathering intensity. Values of CIW range from 73 to 81. In comparison to the calculated CIA values the CIW values are much higher, probably indicating an enrichment of potassium during diagenesis. However, it was shown by Fedo et al. (1995) that CIW tends to be systematically higher than CIA, because it does not reflect the original K/Al ratio of potassium feldspars, which frequently occur in the samples of the palaeosol. Nevertheless, diagenetic potassium enrichment is much likely. In conclusion, the CIA values of the palaeosol are probably slightly higher than calculated, but not as high as the CIW values. The CALMAG values range from 76 to 85 and are therefore higher than the values of CIA and CIW, which is a typical trend (Nordt and Driese, 2010). The clear deviation compared to CIA and CIW values shows that it seems not to be a representative indicator for the investigated type of palaeosol, which is poor in clay minerals.

4.2.3. Estimation of mean annual precipitation (MAP)

For MAP estimation different equations derived from CIA and CIW based on empirical data of the Bw and Bt horizons (Sheldon et al., 2002), were used. Additionally, two further methods are presented and discussed using the total soil iron portion (Stiles et al., 2001), and the CALMAG, which is based on datasets from vertisols (Nordt and Driese, 2010).

$$\text{Nordt and Driese (2010)}: \quad \text{P(mm a}^{-1}) = 22.69\,\text{CALMAG} - 435.8 \quad R^2 = 0.90;\ \text{Standard error}: \pm 108\,\text{mm} \tag{5}$$

$$\text{Sheldon et al. (2002)}: \quad \text{P(mm a}^{-1}) = 221.1\text{e}^{0.0197(\text{CIA-K})} \quad R^2 = 0.72;\ \textit{Standard error}: \pm 181\,\textit{mm} \tag{6}$$

$$\text{P(mm a}^{-1}) = 259.3 \ln\left(\frac{\sum \text{Bases}}{\text{Al}}\right) \quad R^2 = 0.66;\ \text{Standard error}: \pm 235\,\text{mm} \tag{7}$$

$$\text{P(mm a}^{-1}) = 14.265(\text{CIA-K}) - 37.632 \quad R^2 = 0.73;\ \textit{Standard error}: \textit{n.a.} \tag{8}$$

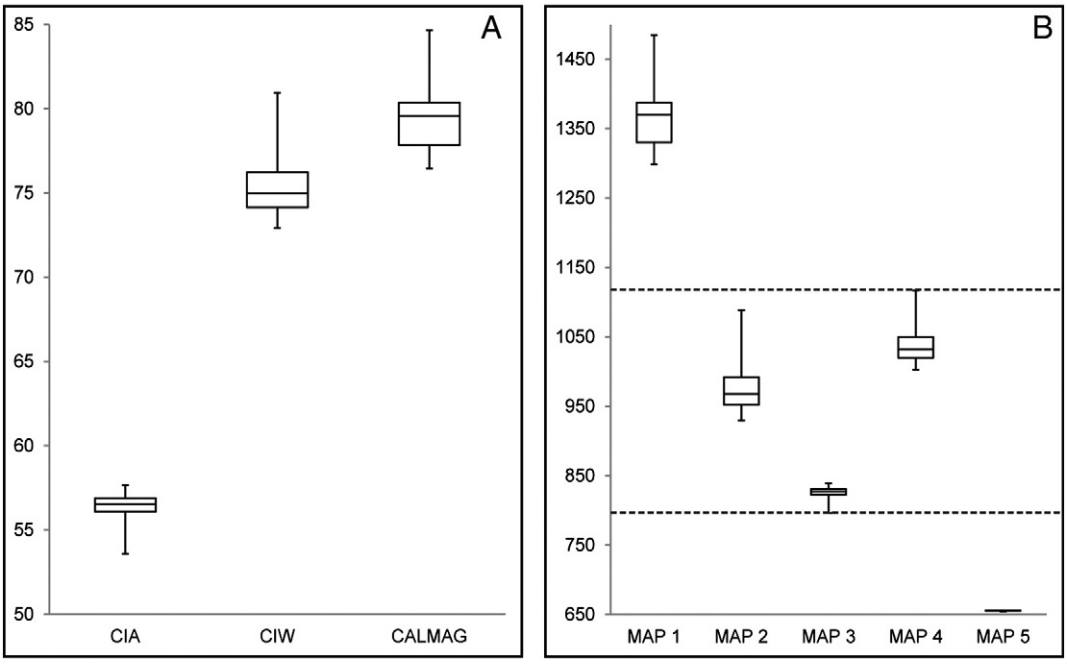

Fig. 8. Boxplot diagrams of geochemical weathering indices and equations of mean annual precipitation. Data source is given by samples from Unit S 6.7 taken from the whole excavation area (n = 13). (A) Comparison of different chemical weathering indices. (B) Most probable range of mean annual precipitation shown by dashed lines derived from various equations (MAP 1 after Nordt and Driese (2010), based on CALMAG; MAP 2–4 after Sheldon et al. (2002), based on CIW; MAP 5 after Stiles et al. (2001), based on total iron portion).

$$\text{Stiles et al. (2001)}: \quad P(\text{mm a}^{-1}) = 654.4 + 31.5\,Fe_{(TOT)} \quad R^2 = 0.92;\ \text{Standard errror}: n.a. \tag{9}$$

By regarding the equations of Sheldon et al. (2002), precipitation values vary between 800 and 1100 mm/a (Fig. 8B). Considering that CIW values are probably lower than calculated, it must be assumed that MAP was likewise slightly lower than estimated. The equation based on total iron content (Stiles et al., 2001) offers much lower values of around 655 mm/a. This is outside of the range of 800–1500 mm/a, for which this equation is valid. So, it seems not applicable to the studied palaeosol. The same seems to be likely for the equation derived from CALMAG, which delivers values from 1300–1480 mm/a. As mentioned before, the CALMAG was developed for vertisols and therefore its application to the analysed palaeosol is limited. Altogether, it can be assumed that palaeoprecipitation rate was likely in a range of 800–1100 mm/a, with a tendency to slightly lower values. One major problem in estimating palaeoprecipitation values at the Hilbersdorf excavation site is the fact that the investigated palaeosol exhibits a low maturity lacking a typical Bt horizon. The low maturity is also indicated by similar CIA values of horizons S 6.6 and S 6.7. Following Sheldon et al. (2002), Sheldon and Tabor (2009) and Adams et al. (2011), the applied methods for providing palaeoprecipitation values are not appropriate under these preconditions. Thus we specify our values in a wider range and by use of different methods. The range of MAP is in agreement to the estimated MAP values derived from depth of carbonate horizon, although it confirms a trend towards slightly lower values.

4.3. Adaptation strategies of plants to palaeoenvironmental conditions

Plants are directly exposed to their environment and therefore more or less adapt to different conditions. Styles of adaptations are manifold encompassing plant architectural modifications of individual organs such as stems, roots and shoots. Moreover, woody tissues usually record any environmental changes in the cellular detail. To amplify our palaeoenvironmental studies we present data from several *in-situ* plants with regard to the architecture of their root systems as well as variations in the tissue of long-lived woody plants.

4.3.1. Evidence from root systems of the in-situ plant community

Palaeosols can be understood as trace fossils of ecosystems, rather than of species or individuals (Retallack, 1999), because they usually do not reveal which kind of trees were involved in their formation. At Hilbersdorf excavation site, however, the T^0 assemblage allows for recognising the kind of plants rooting in the underlying palaeosol.

Fossil *in-situ* rooting systems have been recognised from all major constituents of the ancient plant community at the Hilbersdorf excavation site, including medullosan seed ferns (35%), cordaitaleans (30%), psaroniaceous tree ferns (22%) and calamitaleans (13%) ascertained from 37 stems (altogether 53 stems, 30% remain unidentified) still standing in growth position in an area of 24 x 18 m (Rößler et al., 2012b). According to the extent of secondary growth in their stems, branches and roots of cordaitaleans and calamitaleans seem to represent the older *in-situ* vegetation elements reaching stem diameters up to 0.5 m, although successional patterns in the habitat remain to be evaluated.

Root systems of the upright-standing plants are differentially silicified and often remained in cast preservation. Silicification, in contrast to the frequent fluoritisation in overlying pyroclastics, is the only form of petrifaction inside the palaeosol and mostly incomplete and restricted to larger portions of the root systems. Only in a few cases we recognised detailed preservation down to cell structures. Silicified roots are mostly fragmented, which sometimes made their recovery nearly impossible. Except for the tree ferns, whose roots are exclusively preserved as flattened impressions, root systems of nearly all present plant groups were affected by silicification. For many specimens it was not possible to reconstruct their complete root systems due to the lack of adequate preservation and missing organ connections. In general, the preservation potential seems to decrease with decreasing plant size (Rößler et al., 2014). The uppermost part (0–0.30 m) of the palaeosol profile exhibits the majority of root masses. Most of the specimens have a rooting depth of 0.10–0.25 m, some reach a maximum depth of 0.40 m. The cordaitalean trunk KH0018 represents an exception with a maximum rooting depth of 0.70 m.

Description is done separately for every plant group because architectural features of the root systems are plant group-specific.

4.3.1.1. Medullosan seed ferns. At the Hilbersdorf excavation site seed ferns represent the most abundant plant group, indicated by different traits of stem anatomies, ovules or pollen organs (Feng et al., 2014; Rößler et al., 2012b). In spite of the restricted area a considerable diversity of medullosan seed ferns seems to have grown close together. So far, two forms were identified to intraspecific level, *Medullosa stellata* f. *stellata* and *Medullosa stellata* f. *lignosa* (Rößler et al., 2012b); the presence of several additional species or distinguishable growth forms is likely. The preservation state of their tabular root systems varies from very poor (only relicts of sediment casts) to fairly good (mainly silicified) and seems to depend on trunk diameter, whereby rarely occurring large specimens have partly silicified root systems, e.g., KH0056, KH0124 and KH0198 (Fig. 9A–C). These three specimens have a tap root that departs from the stem base and penetrates vertically into the palaeosol (Fig. 9B). It remained in a silicified state down to 0.25–0.35 m depth and shows appendages to small-sized secondary roots in all three specimens, which are mostly not anatomically preserved. Originating from the stem base, horizontally or slightly obliquely partly silicified secondary roots extend into the upper palaeosol. In KH0124, these secondary roots possess diameters between 0.05 and 0.07 m and a maximum length of 0.80 m (Fig. 9C). In KH0056, secondary roots spread from the stem base in a radius of 1.10 m. Other specimens do not show any relicts of a vertical central root. Instead, several roots extend obliquely from the stem base into the palaeosol, e.g., in KH0050, where roots are partly silicified. The same propagation pattern can be assumed for the non-silicified specimens. It is likely that medullosan seed ferns, according to their species diversity, exhibit at least two different types of root systems, one with a characteristic tap root and another without.

4.3.1.2. Cordaitaleans. Root systems of three specimens were investigated. The best preserved is KH0018, which is nearly completely silicified (Fig. 9D–F). Projecting downward from the 0.45 m wide basal stem, a 0.70 m long, a conical tap root penetrates vertically into the palaeosol. It ends slightly above the massive groundwater calcrete (S 6.4), which could have acted as a natural obstacle (Fig. 9F). From the central stem base, additionally three first-order roots spread nearly horizontally in a radius of c. 1.50 m and a depth of less than 0.40 m. Distally, they branch at least up to second order. One of the roots exhibits an unusual U-turn by first continuing upwards and then in the opposite direction towards the stem base (Fig. 9E). A fourth first-order root steeply penetrates into the palaeosol. Numerous smaller roots, observed in the vicinity of the stem base, either originate from the tap root or do not reveal traceable organ connections.

Two additionally investigated specimens, KH0073 and KH0171, are much smaller than KH0018 and exhibit less completely developed root systems. KH0073 has a silicified vertical tap root originating from the 0.12 × 0.14 m wide stem base. The tap root shows appendages of secondary roots; the latter are not preserved. Furthermore, some roots preserved as flattened impressions spread radially from the stem base, slightly beneath the palaeosol surface. The root system of KH0171 was not silicified. Instead, some root impressions were found spreading from the 0.05 m wide stem base, showing that the degree of silicification

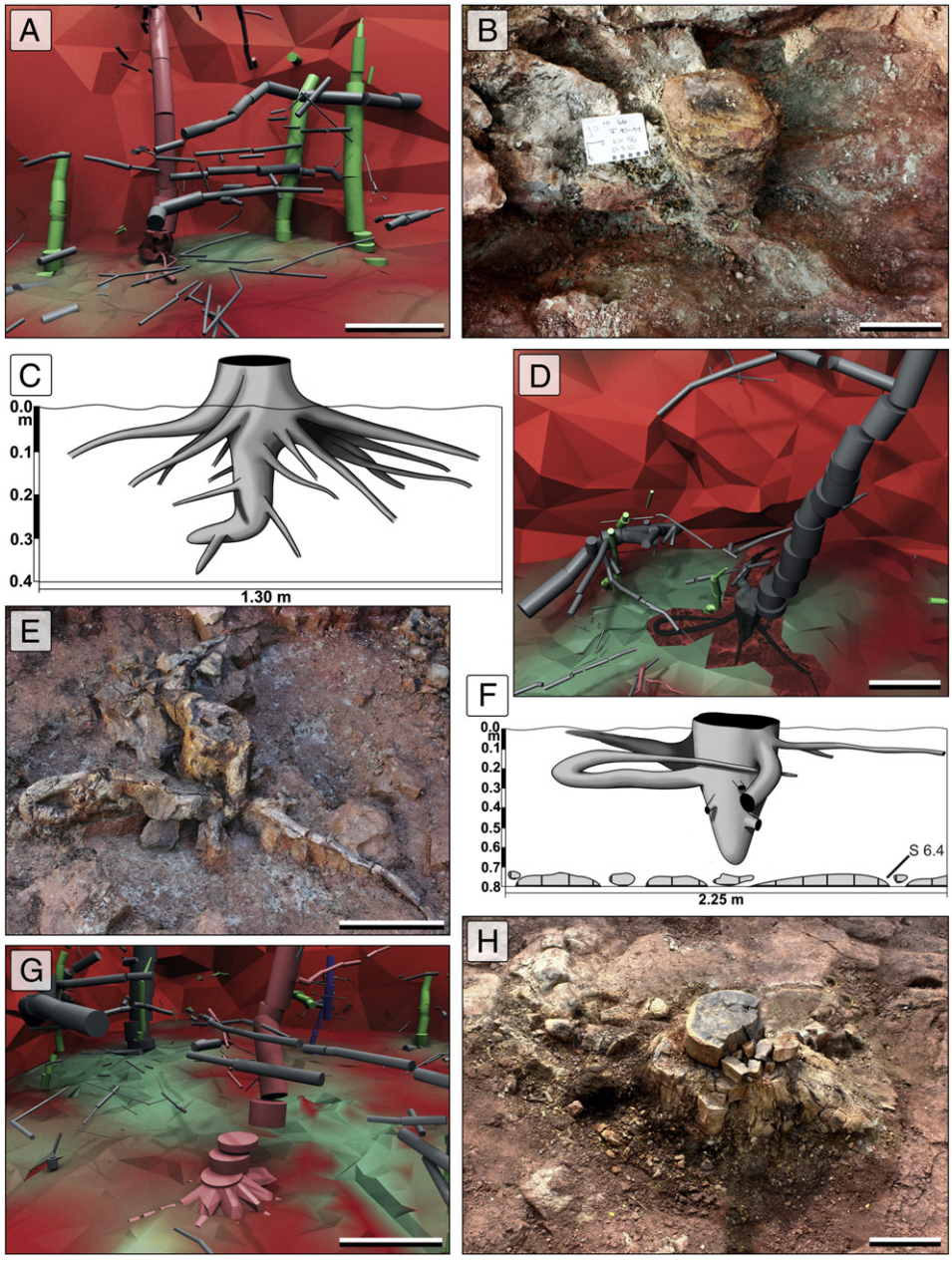

Fig. 9. Root systems of different plant groups. (A) Part of a 3D computer model showing three medullosan seed ferns (green coloured, from left to right: KH0198, KH0124, KH0056) in upright position and rooting in the palaeosol (scale bar: 1 m). (B) Silicified central, conical-shaped root of KH0056 (*M. stellata*, scale bar: 0.1 m). (C) Reconstructed root system of specimen KH0124 (*Medullosa* sp.) showing a central root and numerous obliquely dipping radial roots. (D) 3D computer model of a cordaitalean found in upright position (KH0018); Root system is visualised by cutting the palaeosol surface (scale bar: 1 m). (E) Exposed silicified root system of KH0018 showing four major roots dipping sub-horizontally, whereas one of them exhibits a 180° turn (scale bar: 0.5 m). (F) Reconstructed root system of KH0018 showing a conical shaped central root additionally to the four horizontal roots. Central root does not penetrate the groundwater calcrete (S 6.4). (G) 3D computer model focusing on the basal trunk of an upright standing calamitalean (KH0277, red coloured, scale bar: 1 m). (H) Silicified basal trunk and root system of KH0277 *in-situ* preserved on a cordaitalean deadwood (scale bar: 0.2 m).

seems to be likely a function of tree size. Small specimens could represent juvenile plants, which have poorly developed root systems and therefore seem to be unsuitable for anatomical preservation.

4.3.1.3. Psaroniaceous tree ferns. Psaronius is a well-known genus at the Chemnitz Fossil Lagerstätte (Cotta, 1832; Rößler, 2000), and at the Hilbersdorf excavation site it was an abundant constituent of the former plant community. Slender stems are surrounded by a downward thickening mantle of aerial adventitious roots, a typical feature in many ancient and modern tree fern species (Christ, 1910; Taylor et al., 2009). These endogenously arising secondary roots are produced throughout the whole life of the fern as the stem grows, and have essential mechanical and physiological functions, i.e., anchorage, stability and the uptake of water and nutrients.

Although a considerable local species diversity of psaroniaceous tree ferns is suggested by historical finds from Hilbersdorf (Sterzel, 1918), only distichous specimens like *Psaronius* cf. *simplex* were identified at Hilbersdorf excavation site. The root systems are exclusively preserved as drab-haloed, flattened impressions in the palaeosol (Fig. 10C). Three *in-situ* standing trunks (Fig. 10A) exhibit numerous small vertical to sub-vertical root tubes penetrating the uppermost palaeosol (Fig. 10D). Their marginal roots extend horizontally and spread radially to form a nearly circular root mass of 1 to 2 m in diameter (Fig. 10B). Single roots show an internal

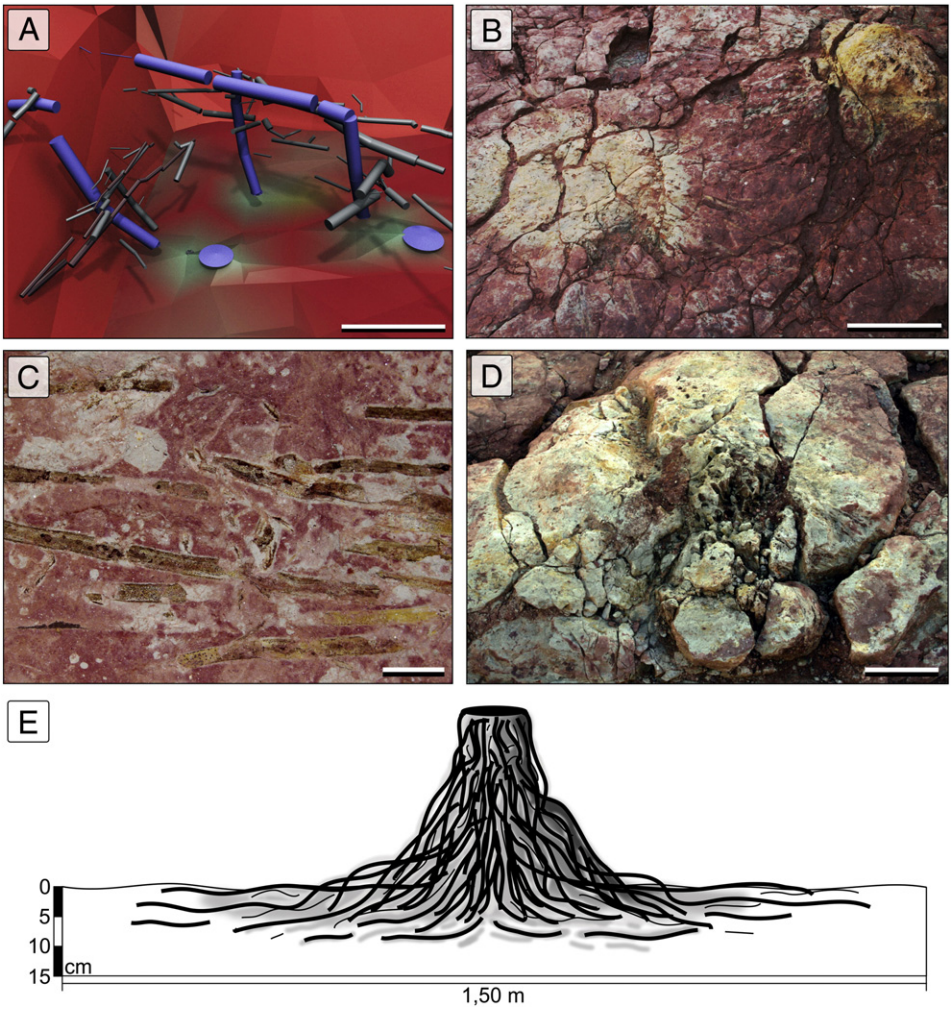

Fig. 10. Morphological features of psaroniaceous tree fern root systems. (A) Three upright standing specimens (blue coloured, from left to right: KH0066, KH0111, KH0117), broken in a height of 1 m and displaced from their stem bases (blue cylinders) by sub-recent slope gliding (scale bar: 1 m). (B) Stem bases of KH0111 (left) and KH0117 (right) show radial spreading of horizontally dipping roots (preserved as drab-haloed traces) and bulging of the palaeosol in the case of KH0117 (scale bar: 50 mm). (C) Horizontally deflected unbranched roots of KH0066, slightly below palaeosol surface (scale-bar: 20 mm). (D) Bleached palaeosol surface below the stem base of KH0066(-09) showing numerous vertical root tubes (scale bar: 50 mm). (E) Reconstruction of the root system of KH0111 showing shallowly spreading roots.

fringe pattern, which is likely due to compaction of the former root tube. Most of them continue straight, and rarely show any branching. The general rooting depth of these tree ferns is not more than 0.25 m (Fig. 10E). At the site of several specimens (e.g., KH0066 and KH0117), the palaeosol surface is considerably elevated, forming a circular hummock (Fig. 10B). The formation of these bulges is still a matter of debate, but probably a result of sediment capture within the basal root mantle. All things considered psaroniaceous tree ferns at the Hilbersdorf excavation site show a shallow-rooting pattern, most of the roots occur only in the uppermost soil layer.

4.3.1.4. Calamitaleans. As indicated by several specimens, the calamitaleans represent free-stemmed, high rising, multiannual trees and exhibit a system of plagiotropic roots with considerable secondary growth. Two well-preserved specimens of *Arthropitys bistriata* (KH0042 and KH0277) are described in detail by Rößler et al. (2014), who provided the earliest unequivocal records of anatomically preserved *in-situ* rooted Permian calamitalean trunks that challenged the traditional reconstructions showing arborescent sphenopsids exclusively as rhizomatous trees. Rößler et al. (2014) presented multiple evidence of organic connection of the stems to their underground root systems. It was demonstrated that *A. bistriata* grew as a free-stemmed tree that was anchored in the soil by numerous secondary roots arising from different nodes of the slightly enlarged trunk base, branching several times and tapering on their oblique downward course. In detail, KH0042 has a basal stem diameter of 0.30 × 0.24 m and ends abruptly at the palaeosol surface. Attached to the stem, six silicified first-order roots of similar diameter extend obliquely into the palaeosol by showing second- and third-order branching. Silicification of roots is restricted to a maximum length of 0.40 m, whereas the distal parts continue as sediment casts. In the vicinity of the trunk, several further silicified roots were documented, but miss a clear connection to a stem. First- and second-order roots show secondary growth and belong to the common *Astromyelon* type. Asymmetrical growth-ring-like tissue density variations were observed. KH0277 (Fig. 9G–H) shows a similar root system to that of KH0042, but in contrast was growing upon a cordaitalean deadwood trunk. From the 0.32 × 0.40 m wide basal trunk seven first-order roots with a maximum length of 0.65 m depart obliquely into the palaeosol down to a maximum depth of 0.40 m. They show a thickened, conical habitus and attachments of second-order roots arranged in node-like levels. Roots mainly be of

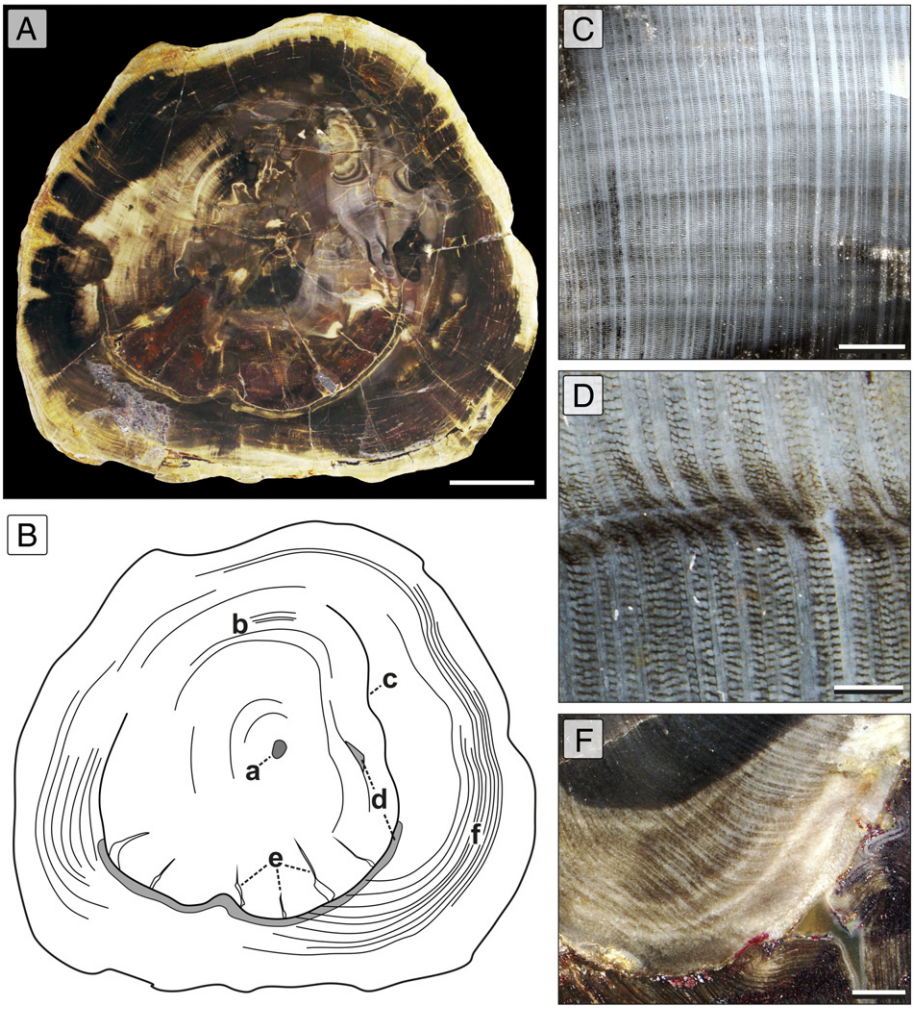

Fig. 11. Tissue density variations in the wood of an *in-situ* calamitalean from Hilbersdorf excavation site (*A. bistriata*, KH0277). (A) Transverse section from the base of KH0277-04 showing tissue density variations and preservational variation visible by changing colours (scale bar: 50 mm). (B) Documentation of tissue density variations in the section of "(A)": a—pith, b—zone of irregular tissue density variations (see also "(C)"), c—non-circumferential, but very distinct tissue density variations or event zone (see also "(D)"), respectively, which is associated to a major injury to the outer part of the trunk, d—callus tissue, overgrowing injuries from two sides (see also "(E)"), e—radial fissure cracks caused by wood contraction, f—zone of regular tissue density variations (C) Irregular tissue density variations with predominantly gradational cell size variation (scale bar: 1 mm). (D) Distinct event zone showing decrease of cell size and cell deformation (scale bar: 0.5 mm). (E) Zone of major injury of the event zone showing a fissure crack in the inner wood, overgrown by callus tissue from the right (scale bar: 2 mm).

the *Astromyelon* type, in one case assignable to the *Asthenomyelon* type, as well. A high amount of ray parenchyma inside the wood, approximately 50%, is conspicuous, but corresponds well to calamitalean aerial parts.

4.3.2. Evidence from woody arboreal plants: growth rings?

Wood structure and composition have been investigated since the early days of plant anatomy, and most living woody species have been described in great anatomical detail (e.g., Richter et al., 2004; Schweingruber et al., 2011; Wheeler et al., 1989, 2007). Nevertheless, despite of the long history of plant anatomical investigations, palaeoecological knowledge about most Palaeozoic species, even frequently occurring ones such as calamitaleans, cordaitaleans or medullosan seed ferns, remains superficial. Although there are a few helpful publications that enlighten the influence of environmental factors on the wood structure of both living and fossil trees (Chaloner and Creber, 1990; Creber and Chaloner, 1984), a general assignment of the substantial knowledge provided by the study of modern trees (Schweingruber et al., 2008, 2011) to arboreal plants from the fossil record is restricted to selected applications (Ash and Creber, 1992; Falcon-Lang, 1999, 2003, 2005; Francis, 1984). If vegetation can be called "crystallised climate" as was metaphorically expressed by Köppen (1936), plants with considerable secondary growth epitomise this in particular.

However, even with a local focus one can find significant archives of habitat cyclicity, e.g., in persisting vegetation elements. Extending the vegetative life span of *Arthropitys ezonata* ensures that it may have had the capacity to survive unfavourable periods and extend its reproductive life span, including during such less favourable times (Rößler and Noll, 2006). Whilst adaptation to seasonal drought is well understood in evolutionarily derived plants, such as conifers or cycads, we found a number of survival strategies also amongst more primitive clades. Based on palaeofloras from different low-latitude sites of both Euramerica and Gondwana we can adduce that phenotypic plasticity amongst arboreal sphenopsids and psaroniaceous tree ferns enabled them to withstand severe moisture stress (Barthel and Weiß, 1997; Neregato et al., 2015; Rößler and Noll, 2006, 2010; Tavares et al., 2014). Although both are usually regarded as

evolutionarily less-derived plant lineages, we recognise trends to enlarge the water storage capacity by more voluminous parenchyma portions or reduce transpiration by protecting leaves with a cover of fine hairs, reducing their surface or simply by shedding leafy shoots during drier seasons.

At first view, "growth" rings in calamitaleans sound strange, ultimately these pteridophytes are presumed as typical representatives of Palaeozoic wetland communities showing long-term compositional conservatism and likewise colonising wet clastic-substrates or mires (Falcon-Lang, 2015). On the other hand calamitaleans can exhibit considerable secondary growth (Rößler and Noll, 2006; Rößler et al., 2012a) offering a local monitoring of environmental conditions over longer periods of time. Different organs of the woody arboreal plants, calamitaleans in particular, exhibit various patterns of tissue density variations in their secondary xylem.

4.3.2.1. Tissue density variations in calamitaleans. Amongst tissue density variations we recognised several types of growth interruptions by investigating two calamitalean specimens. One of them (*Arthropitys bistriata*, KH0277-04, Fig. 11) was found in growth position, the other (*A. sterzelii*, K3257) is from the vicinity of the Hilbersdorf excavation (Fig. 12). The transverse section of the basal part of the stem (KH0277-04) measures 310 × 220 mm. Cell preservation differs within the section of KH0277, whereas in K3257 cells are uniformly well-preserved. The major type of tissue density variations, predominant in both specimens, is characterised by diffuse radial zones of slightly smaller and thick-walled cells, quite comparable to false rings (Creber and Chaloner, 1984; Figs. 11C/D and 12C). Most are circumferential and parallel to each other. The ring width of tissue density variations varies considerably; intervals are wider and more irregular in the central part of the stems, but narrower and more regular in the marginal part (Fig. 11B). Some of the more distinct tissue density variations show a gradual decrease of cell size and increase of cell wall thickness followed by a thin zone of deformed, crushed or collapsed cells, accompanied by disruption of normal growth direction of the tracheids (Fig. 11D). Frequently so called 'double rings' occur (e.g., Francis, 1984). Exceptional tissue density variations are present in KH0277-04 and K3257. In KH0277-04 such a zone is represented by a very clear, but non-circumferential tissue density variations characterised by sudden cell size decrease and deformation of cells followed by a distinct "recovery phase" back to normal cell growth (Fig. 11B, D). The radial section of this tissue density variation is interrupted by a prominent scar associated with fissure cracks resulting from an outer injury, which is followed by a prominent zone of callus tissue growing from both sides of the scar (Fig. 11B, E). In K3257, an exceptional zone appears by a gradual cell wall thickening and cell size decrease followed by a thin zone of crushed cells and a sudden growth of large thin-walled parenchyma (Fig. 12E, F).

4.3.2.2. Interpretation. The majority of tissue density variations found in the investigated specimens are different from normal growth rings usually occurring in woody trees of temperate latitudes. Instead, they represent zones of reduced growth activity as is typical for false rings, frequently observed in the tropics and subtropics as well as in arid desert regions (Chapman, 1994; Creber and Chaloner, 1984; Schweingruber et al., 2008). They likely represent both seasonal and intra-seasonal fluctuations and are probably caused by limiting environmental conditions, such as reduced water availability or frost. Due to the palaeogeographical position of the study area, at approximately 15°N, frost events seem implausible. With regard to the regular ring width pattern in the outer part of the stems, the tissue density variations likely reflect restricted growth during seasonal dry phases. More severe droughts usually led to the formation of zones with collapsed and even crushed cells (Fig. 11D). Ring width variation between the inner and outer parts of the stem is probably due to ontogenetic development. Wide and irregular tissue density variations in the central part suggest fast growth of the young plant, whereas very regular and narrow tissue density variations dominating the outer part of the stem developed in a later growth stage (Schweingruber et al., 2008).

Because of their unique occurrence exceptionally severe tissue density variations occurring in both specimens are seen as 'event zones' being the result of distinct environmental impact. There are several possible causes leading to the formation of event zones, e.g., frost, severe drought, defoliation, wildfires, lightning strikes, volcanic ash falls or flash floods (Byers et al., 2014; Creber and Chaloner, 1984; Schweingruber et al., 2011). Flash floods can be excluded for both specimens according to the sedimentary record. As argued above severe frost events are unlikely. The same for wildfires, because no charcoal was found in the palaeosol. Most likely are severe droughts or even volcanic ash falls; the latter could result from pre-eruption events presaging the major eruption of the Zeisigwald volcano. It is hard to say whether the event zones of KH0277-04 and K3257 were caused by the same environmental event because no correlation is available, so far.

Tissue density variations are not restricted to calamitaleans. They are likely to occur in medullosan seed ferns and cordaitaleans as well, which contributes to their environmental significance. Future research will show to what extent tissue density variations in specimens of different species are useful to recognise short-time climatic developments and how they correlate to the palaeoclimatic model of Roscher and Schneider (2006), which suggests different patterns of seasonality. Altogether, tissue density variations record the most detailed level of environmental rhythmicity in the habitat and therefore possess the same high resolution as the laminated carbonate of the lacustrine Reinsdorf Horizon does.

5. Discussion

5.1. Interregional comparisons of geological and palaeontological background

Traditionally, the major indicators of deep-time palaeoclimate are provided by palaeontological, pedological and geochemical evidence (e.g., DiMichele et al., 2008; Gulbranson et al., 2015; Hasiotis et al., 2007; Raymond et al., 2014; Tabor and Poulsen, 2008). Data presented above shed light on the Chemnitz Fossil Forest's palaeoenvironment, demonstrating that a seasonal climate influenced palaeosol formation, geochemical parameters and plant growth. Provided that an adequate stratigraphic control exists (Roscher and Schneider, 2005; Schneider and Romer, 2010; Schneider et al., 2014), reconstructions of palaeoclimate and palaeogeography are of particular interest (Isbell et al., 2012; Peyser and Poulsen, 2008; Roscher and Schneider, 2006; Sahney et al., 2010; Schneider et al., 2006; Tabor, 2013). Several approaches have been proven to be very useful for providing palaeoclimatic data, such as palaeobotany, palaeopedology and geochemistry (Bomfleur and Kerp, 2010; Cecil et al., 2014; DiMichele et al., 2008, 2011; Rosenau et al., 2013; Schneider et al., 2006; Sheldon and Tabor, 2009; Tabor and Poulsen, 2008; Wang et al., 2014). Recently the type of organic matter obtained from humic coals and limnic sediments of Pennsylvanian to Permian basins was determined using organic petrology; Rock-Eval data and biomarker distribution support much higher climatic variability when cycled through a wet/dry tropical state (Izart et al., 2012). However, irrespective of a few dispersed and highly carbonised particles in petrified wood, organic matter is unfortunately not preserved at the Chemnitz site (Wittke et al., 2004). Nevertheless, there are other promising circumstances featuring this fossil Lagerstätte (Rößler et al., 2012b). The extensive fossil record of this T^0 assemblage, which characterises the Chemnitz Fossil Forest as a unique window into the northern Pangaean Cisuralian, and additional information from the palaeosol sustaining this forested habitat underline a certain phase of increased humidity. The dense, multi-aged hygrophilous vegetation and its relations to a number of terrestrial animals characterising this mineral soil lowland environment fits with the wet phase D around 290 Ma of Roscher and Schneider (2006).

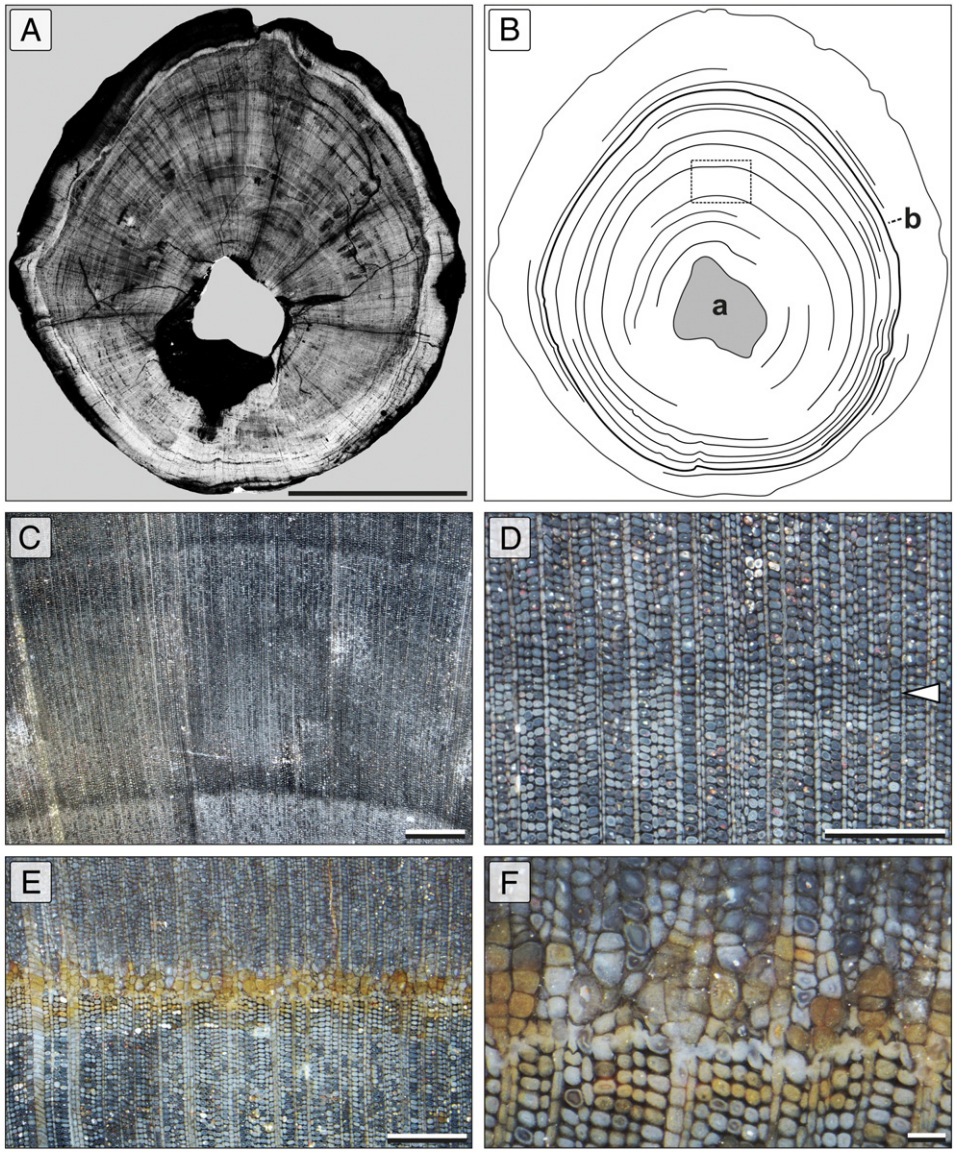

Fig. 12. Tissue density variations in a calamitalean (*A. sterzelii*, K3257) from the vicinity of the Hilbersdorf excavation. (A) Transverse section showing tissue density variations and uniformly well preserved wood (illustrated in negative black/white image, scale bar: 50 mm). (B) Documentation of visible tissue density variations forming a regular pattern of mostly circumferential zones. a—pith cavity, b—distinct event zone; Dashed square—part of "(C)" (scale bar: 50 mm). (C) Typical regular tissue density variations showing considerable ring width (scale bar: 1 mm). (D) Detail of the lower tissue density variation in "(C)" characterised by a slight and gradational decrease of cell size and an increase of cell wall thickness (arrow, scale bar: 0.5 mm). (E) Event zone marked in "(B)": The zone is accompanied by colour variations (scale bar: 0.5 mm). (F) Detail of "(E)" characterised by a decrease of tracheid size and increase of cell wall thickness, followed by a zone of collapsed cells and an initial growth of thin-walled large-celled parenchyma from the rays (scale bar: 0.1 mm).

Accompanying the general aridisation trend of equatorial Pangaea (Chumakov and Zharkov, 2002; DiMichele et al., 2006; Tabor, 2013; Tabor and Poulsen, 2008) and a substantial rise in atmospheric CO_2 (Peyser and Poulsen, 2008), a repeated change of several dry and wet phases is evidenced, based on sophisticated multi-method stratigraphic evaluations, including well-founded correlations amongst several European and North-American late Palaeozoic basins and to the Southern hemisphere Karoo Basin (Schneider et al., 2006). The global warming from the Carboniferous icehouse into the Mesozoic greenhouse exhibits much variation at different temporal and spatial scales (Looy et al., 2014; Montañez and Poulsen, 2013; Torsvik and Cocks, 2004). As depicted by DiMichele (2014), the distribution of equatorial wet and seasonally dry biomes and their vegetation types oscillated according to glacial–interglacial climatic cycles; as these responded to environmental disturbances they may have recorded both trends and controls within Pangaean tropics. One of the most striking palaeoclimatic patterns is the appearance of seasonality caused by the shift of the Intertropical Convergence Zone (ITCZ) over the equator (Kutzbach and Ziegler, 1994; Roscher and Schneider, 2006). Evidence of seasonality received recently special attention from different directions, e.g., the development and changes in fluvial architecture (Allen et al., 2014), fossil plant anatomy (Neregato et al., 2015; Rößler et al., 2014) and spatial–temporal biome dynamics (Looy et al., 2014).

The overall climatic fluctuation of wet and dry phases was not only determined by global-scale influences, such as orbital and consequently glacio-eustatic cycles according to the waxing and waning of the Gondwanan icecap, plate tectonics, palaeogeography, and oceanic currents, but these effects were additionally modified by regional-scale influences, like volcanotectonic activity and sediment delivery dependent on the geomorphic situation and drainage patterns. According to its isotopic age (see above) and biostratigraphic indications (Schneider and Werneburg, 2012) the Leukersdorf Formation belongs to the wet phase D of Roscher and Schneider (2006), roughly between 292 and 289 Ma. Each of these wet phases recognised since the late Westphalian (Moscovian) is drier than the previous one. The floral associations accompanying the Permian wet and dry phases in Central

Europe are characterised by Barthel and Rößler (2012). Late Pennsylvanian/early Permian (Gzhelian/Asselian) wet phase C is represented in most, if not all, Central European basins by basin-wide distributed grey facies and common coal seams, e.g., the famous Manebach Formation in the Thuringian Forest Basin (Barthel and Rößler, 1997). This flora is generally dominated by peat-forming hygrophilous elements and species-rich hygrophilous to mesophilous fern and pteridosperm associations on peat or mineral substrates. In the dry phase between wet phases C and D, wet red beds interchange with the grey facies of the lake levels and coals are lacking. The flora of the lake levels is characterised by mesophilous to xerophilous associations with rare occurrences of hygrophilous elements from the near-lake surroundings. In the wet phase D the last perennial lakes occur in all European basins. Only in single basins peat-forming facies re-occurred, as indicated in the Buxières Formation of the Bourbon l'Archambault Basin of the French Massif Central (Roscher and Schneider, 2006).

In the early wet phase D lake sediments are still dominated by clastics, later and depending on basin configuration and lake size, these lake sediments show increasingly carbonates. The latter is exemplified by microbial-mat-dominated lake and pond carbonates of the Niederhäslich Limestone Horizon of the Döhlen Graben, about 50 km east of the Chemnitz Basin (Schneider, 1994), and likewise by lacustrine carbonate laminites found in the upper Oberhof Formation in both grey and red facies (Lützner et al., 2012; Schneider and Gebhardt, 1993). Generally, a dual lamination is well developed in pelagic lake sediments of this time interval. Ideally, the varve-like clastic couplets consist of a basal silt lamina followed by a darker, C_{org} enriched clayish lamina; carbonate couplets consist of a darker lamina enriched in clastic components and C_{org} and a bright, nearly pure carbonate lamina. Transitions between the couplets are gradually, irregularities can be common. The Reinsdorf Carbonate Horizon of the Leukersdorf Formation, about 30 m below the Zeisigwald Tuff, consists of one to five limestone beds, which document the facies and distribution of the lake and pond environment (Schneider et al., 2012). The common facies type is a monotonous grey micritic gastropod-ostracod limestone; towards the basin centre carbonate laminites with marl-limestone couplets are developed. Moreover, evaporites as pure dolosparites and gypsum are additionally reported from the Reinsdorf Carbonate Horizon (Schneider et al., 2012). Altogether this points to alternating wet and dry seasons and an increasing aridity during the wet phase D.

At the time of growth and burial of the Chemnitz Petrified Forest, the sediments of the Leukersdorf Formation representing the surrounding forested area, and those below and above this level, are wet red beds. The depositional environment is reconstructed as an alluvial fan and braidplain system (Schneider et al., 2012). Red siltstones and silty sandstones as overbank deposits of intermittent fluvial discharge and stacked and amalgamated distal sheet-flood deposits predominate in the basin centre. Typical are metre-thick vertisols and decimetre- to metre-thick calcisols of different maturity up to mature calcretes and dolocretes. The formation of the latter calls for precipitation rates not exceeding about 600 mm/a and extended dry seasons (Jäger, 1939; Wright, 1987, 1992). *Scoyenia*- and *Planolites montanus*-type bioturbation are common. The frequent occurrence of *Scoyenia* indicates fluctuating groundwater levels; whitish-greenish leached coarser channel clastics intercalated with red siltstones indicate a certain amount of groundwater flow. However, remains of vegetation apart from milimetre-sized fine horizontal roots, centimetre-thick rhizoconcretions and rare walchian twigs are missing in the wet red beds. Regarding its palaeolatitudinal position of about 15°N and its climate sensitive litho- and biofacies this environment could be interpreted as a nearly unvegetated tropical, semi-arid biome with evaporation exceeding precipitation.

The Chemnitz Fossil Forest appears to contradict this interpretation. The geology of the Chemnitz Basin in general and the Leukersdorf Formation in are very well established by detailed geological mapping since the mid-19th century and detailed investigations of several thousand metres of drilling cores (Schneider et al., 2012). Traces of a vegetated area comparable to this spatially restricted but diverse forest ecosystem have not been found in this formation. Likewise, such a complex palaeosol horizon, on which the forest developed, was not recognised anywhere throughout the Leukersdorf Formation. Therefore, the key to resolving this contradiction probably lies in the palaeosol.

5.2. Palaeoclimatic and environmental significance

Palaeosols have proven remarkably useful for examining a set of geological questions concerning palaeoclimatic studies, such as the estimation of palaeoprecipitation rates (Caudill et al., 1996; Retallack, 1994, 2005), palaeotemperatures (Tabor and Montañez, 2005), changes in atmospheric composition (Tabor and Poulsen, 2008), calculation of aggradational and subsidence rates (Sheldon and Retallack, 2001), reconstructions of ancient landscapes and basin development histories, and stratigraphic applications at different spatial scales (e.g., Kraus, 1999; Lu et al., 2015; Mack et al., 2010).

The relationship between the depth to a specific nodular soil horizon and the annual precipitation was first expressed by Jenny (1941) and offers a useful pedogenic indicator for interpreting aridland soils. Based on carbonate horizons (Nordt et al., 2006; Retallack, 1994, 2000, 2005) and gypsic horizons (Retallack and Huang, 2010) it was proven to be appropriate to estimate palaeoprecipitation also from palaeosols, once the depth to the nodular horizon is corrected for compaction. Although challenged by Royer (1999) this relationship seems to be largely feasible as a quantifying climofunction and yields, applied to the calcrete at the Hilbersdorf excavation, a realistic value of 812 $\pm$ 147 mm/a, which is in agreement with the range of 800–1100 mm/a that is confirmed by molecular weathering indices.

The Variscan Orogen did not result in an orographic east–west barrier, and accordingly the Inter-Tropical Convergence Zone was widely displaced, causing four seasons (dry summer/winter, wet spring/autumn) at around 300 Ma in the palaeoequatorial belt (Roscher and Schneider, 2006), implicating a monsoonal circulation pattern (Roscher et al., 2008, 2011). Considering the aforementioned palaeosol characteristics, with mixed carbonate/ferric glaebules, comparisons to regions now having a monsoonal climate (Courty and Fédoroff, 1985; Sehgal and Stoops, 1972) seems justified. However, the growth ring-like record, especially that found in woody calamitaleans does not allow further refinement of the climatic evidence, in particular for determining the number of seasons. Nevertheless, the kind of habitat cyclicity documented in more or less clear tissue density variations in all of the arboreal woody plants, for the first time provides the opportunity to implement the fourth dimension within this *in-situ* ecosystem. Future investigations are necessary to evaluate the potential of wood in general and of different woody organs in particular as archives of Permian climate. Groundwater resources, albeit fluctuating, had obviously a major influence at our site in maintaining a dense wet forest that surely buffered moisture availability during seasons. The obvious contradiction of much precipitation on the one hand, and on the other the indication for low chemical weathering, seem to require a strong seasonal regime as proposed by this study. Although the Chemnitz site flora encompasses a considerable portion of stream-side elements *sensu* DiMichele et al. (2006), such as calamitaleans and tree ferns, it shows surprising much conformity with the conservative wetland biome of basinal lowlands characterised by DiMichele et al. (2009) as "Wetland vegetation dominates, with occasional preservation of allochthonous plant remains from the nearest extrabasinal areas." However, initially expected indications of waterlogging, peat formation and short-term preservation are lacking completely. Although woody plants recorded climate sensitive oscillations, we cannot call this localised high-moisture habitat of calamitaleans, tree ferns, medullosan seed ferns and cordaitaleans a seasonally dry assemblage. Typical elements of a seasonally dry biome, e.g., the putative cycadaleans "*Pterophyllum*"

and *Plagiozamites*, occurred much earlier in the Chemnitz Basin (Sterzel, 1918) and are documented from the underlying Planitz Formation. Does the remarkable character of the vegetation community at the Hilbersdorf locality under the reconstructed palaeoclimatic conditions remain controversial? Although, as shown, different plants developed adaptational strategies to survive moisture stress, additional environmental factors may have contributed to the stability of the ecosystem, e.g., a local minor seasonal fluctuation of the groundwater table. This assumption is supported by the occurrence of shallow and mainly horizontally oriented root systems of *in-situ* trees that may have adapted to a high groundwater table (Falcon-Lang et al., 2011; Jenik, 1978; Pfefferkorn and Fuchs, 1991). The presence of tap-root systems as recognised for cordaitaleans and medullosan seed ferns could represent an adaption to a deeper groundwater table during drier seasons. Favoured by site-specific groundwater conditions, the local climatic self-organisation of a hygrophilous forest vegetation community could have buffered its own stability, even within drier surroundings (Schneider et al., 1984). By reflecting local humid micro-environmental conditions, the forest ecosystem could be compared to a "wet spot" *sensu* DiMichele et al. (2006). This is supported by the upper palaeosol section, which shows several similar features as described for the pedotype of the "wet spots" (DiMichele et al., 2006). Summarising the floral composition, environmental and pedological features we see much similarities of the spatially restricted Chemnitz site to the early Permian Sobernheim fossil assemblage in western Germany (Kerp, 1996, 2000; Kerp and Fichter, 1985; Krings and Kerp, 2000) and even to the palaeofloras of low-latitude equatorial Gondwana (Dias-Brito et al., 2007; Rößler, 2006), underlining the sporadical re-appearance of wet biota in the early Permian that is characterised by a general aridification. Floral assemblages from the Permian of northeast Brazil are dominated by stream-side elements of considerable diversity, such different evolutionary lineages of tree ferns, calamitaleans and gymnosperms (Capretz and Rohn, 2013; Kurzawe et al., 2013a,b; Neregato et al., 2015; Rößler and Galtier, 2002a,b, 2003). Although hygrophilous elements are largely prevailing, strong seasonality is evident from specialised drought adaptations of plants (Tavares et al., 2014), frequent growth interruptions in long-living woody plants (Rößler et al., 2014), silcrete palaeosols and gypsite accumulations (Dias-Brito et al., 2007).

In addition to the influence of environmental conditions on the flora, some faunal characteristics of the Chemnitz Fossil Forest ecosystem should be mentioned in this context. Good drainage and a high Eh value in the upper palaeosol were ideal for faunal colonisation. The frequency of terrestrial gastropods down to a maximum depth of 0.40 m, as well as the occurrence of scorpions preserved within their original burrows, a few centimetres below the palaeosol surface indicate adequate living conditions encompassing soil moisture, aeration and nutrient supply in a loose mineral substrate. However, the burrowing behaviour of terrestrial gastropods has never been documented in the Palaeozoic fossil record. Given the seasonally driven moisture stress, burrowing could be interpreted as a survival strategy to prevent from desiccation during periods of drought. Further studies will go more into detail regarding palaeoecological interactions of the substrate, plants and animals.

6. Conclusions

1) The early Permian fossil forest of Chemnitz appears as a spatially restricted and taphonomically favoured "wet spot", surrounded by an obviously almost unvegetated dry environment, characterised by a well-drained alluvial fan/braidplain depositional system proximal to a volcanic vent.
2) The forest ecosystem developed in a low latitude seasonal tropical, semi-humid local to semi-arid regional climate with an estimated annual precipitation in a range of 800–1100 mm.
3) A diverse community of arboreal plants grew on a mineral substrate represented by an immature, entisol-like palaeosol, lacking features of intense chemical alteration, probably due to a relatively short formation time.
4) A long-term stable, but seasonally fluctuating groundwater table in combination with phases of high evapotranspiration led to the formation of a groundwater calcrete, succeeding and overprinting an initial pedogenic calcrete, which formed before the forest ecosystem developed.
5) Seasonality is not only recorded by the co-occurrence and intergrowth of carbonate and hematite glaebules in the palaeosol, but also in long-lived woody plants by forming tissue density variations, which are predominantly similar to modern "false rings". Particular event zones indicate temporary phases of severe environmental stress, probably induced by droughts.
6) Plants adapted to seasonally variable water availability by the formation of shallow voluminous root systems (psaroniaceous tree ferns, calamitaleans) densely penetrating the upper soil horizons. Gymnosperms (cordaitaleans and medullosan seed ferns) show additional formation of low to medium depth tap roots.
7) Besides a diverse plant community, the palaeosol was colonised by several faunal elements such as terrestrial gastropods and arachnids. The entity of organisms preserved at Chemnitz Fossil Lagerstätte includes different vertebrates and arthropods and ultimately reflects a relatively young, but already well-established ecosystem with a remarkably developed trophic pyramid.

Acknowledgements

We highly acknowledge the encouraging support of Thorid Zierold, Mathias Merbitz, Ralph Kretzschmar and Volker Annacker (all Chemnitz) during the ongoing research funded by the German Science Foundation (Project RO 1273/3-1). A special gratitude is addressed to Stanislav Opluštil and his team from the Charles University in Prague for the great offer of comprehensive geochemical analysis and competent support. Further we thank the technical staff from the TU Bergakademie Freiberg for manifold sample preparation. Finally we are grateful to two anonymous reviewers for their helpful and constructive comments or suggestions.

References

Achyuthan, H., Shankar, N., Braida, M., Ahmad, S.M., 2012. Geochemistry of calcretes (calcic palaeosols and hardpan), Coimbatore, Southern India: formation and paleoenvironment. Quat. Int. 265, 155–169.
Adams, J.S., Kraus, M.J., Wing, S.L., 2011. Evaluating the use of weathering indices for determining mean annual precipitation in the ancient stratigraphic record. Palaeogeogr. Palaeoclimatol. Palaeoecol. 309, 358–366. http://dx.doi.org/10.1016/j.palaeo.2011.07.004.
Allen, J.P., Fielding, C.R., Gibling, M.R., Rygel, M.C., 2014. Recognizing products of palaeoclimate fluctuation in the fluvial stratigraphic record: an example from the Pennsylvanian to Lower Permian of Cape Breton Island, Nova Scotia. Sedimentology 61, 1332–1381.
Alonso-Zarza, A.M., 2003. Palaeoenvironmental significance of palustrine carbonates and calcretes in the geological record. Earth-Sci. Rev. 60, 261–298.
Alonso-Zarza, A.M., Genise, J.F., Verde, M., 2011. Sedimentology, diagenesis and ichnology of Cretaceous and Palaeogene calcretes and palustrine carbonates from Uruguay. Sediment. Geol. 236, 45–61. http://dx.doi.org/10.1016/j.sedgeo.2010.12.003.
Arakel, A.V., 1986. Evolution of calcrete in palaeodrainages of the Lake Napperby area, Central Australia. Palaeogeogr. Palaeoclimatol. Palaeoecol. 54, 283–303.
Ash, S.R., Creber, G.T., 1992. Palaeoclimatic interpretation of the wood structures of the trees in the Chinle Formation (Upper Triassic), Petrified Forest National Park, Arizona, USA. Palaeogeogr. Palaeoclimatol. Palaeoecol. 96, 299–317.
Barthel, M., 1976. Die Rotliegendflora Sachsens. Abhandlungen des Staatlichen Museums für Mineralogie und Geologie zu Dresden 24 (190 pp., Dresden).
Barthel, M., Rößler, R., 1997. Tiefschwarze Kieselstämme aus Manebach. Abhandlungen des Naturhistorischen Museums Schleusingen 12 pp. 53–61.
Barthel, M., Rößler, R., 2012. Pflanzen und Pflanzengesellschaften des Rotliegend. In: Lützner, H., Kowalczyk, G. (Eds.), Stratigraphie von Deutschland X. Rotliegend. Part I: Innervariscische Becken. Schriftenreihe der Deutschen Gesellschaft für Geowissenschaften 61, pp. 79–97 (Hannover).
Barthel, M., Weiß, H., 1997. Xeromorphe Baumfarne im Rotliegend Sachsens. Veröff. Mus. Naturkunde Chemnitz 20, 45–56.
Besly, B.M., Fielding, C.R., 1989. Palaeosols in Westphalian coal-bearing and red-bed sequences, Central and Northern England. Palaeogeogr. Palaeoclimatol. Palaeoecol. 70, 303–330.

Birkeland, P.W., 1999. Soils and Geomorphology. 3rd ed. Oxford University Press, New York (430 pp.).

Bomfleur, B., Kerp, H., 2010. The first record of the dipteridfern leaf *Clathropteris* Brongniart from Antarctica and its relation to *Polyphacelus stormensis* Yao, Taylor et Taylor nov. emend. Rev. Palaeobot. Palynol. 160, 143–153. http://dx.doi.org/10.1016/j.revpalbo.2010.02.003.

Brewer, R., 1976. Fabric and Mineral Analysis of Soils. 2nd ed. Robert E. Krieger Pub. Co.; Huntington, New York (482 pp.).

Byers, B.A., Ash, S.R., Chaney, D., DeSoto, L., 2014. First known fire scar on a fossil tree trunk provides evidence of Late Triassic wildfire. Palaeogeogr. Palaeoclimatol. Palaeoecol. 411, 180–187. http://dx.doi.org/10.1016/j.palaeo.2014.06.009.

Canham, C.A., Froend, R.H., Stock, W.D., Davies, M., 2012. Dynamics of phreatophyte root growth relative to a seasonally fluctuating water table in a Mediterranean-type environment. Oecologia 170, 909–916. http://dx.doi.org/10.1007/s00442-012-2381-1.

Capretz, R.L., Rohn, R., 2013. Lower Permian stems as fluvial paleocurrent indicators of the Parnaíba Basin, northern Brazil. J. S. Am. Earth Sci. 45, 69–82.

Caudill, M.R., Driese, S.G., Mora, C.I., 1996. Preservation of a proto-Vertisol and an estimate of Late Mississippian paleoprecipitation. J. Sediment. Res. 66, 58–70.

Caudill, M.R., Driese, S.G., Mora, C.I., 1997. Physical compaction of vertic palaeosols: implications for burial diagenesis and palaeo-precipitation estimates. Sedimentology 44, 673–685.

Cecil, C.B., DiMichele, W.A., Elrick, S.D., 2014. Middle and Late Pennsylvanian cyclothems, American Midcontinent: ice-age environmental changes and terrestrial biotic dynamics. C. R. Geosci. 346, 159–168.

Césari, S.N., Busquets, P., Méndez-Bedia, I., Colombo, F., Limarino, C.O., Cardó, R., Gallastegui, G., 2012. A late Paleozoic fossil forest from the southern Andes, Argentina. Palaeogeogr. Palaeoclimatol. Palaeoecol. 333–334, 131–147. http://dx.doi.org/10.1016/j.palaeo.2012.03.015.

Chaloner, W.G., Creber, G.T., 1990. Do plants give a climatic signal? J. Geol. Soc. 147, 343–350.

Chapman, J.L., 1994. Distinguishing internal development characteristics from external palaeoenvironmental effects in fossil wood. Rev. Palaeobot. Palynol. 81, 19–32.

Christ, H., 1910. Die Geographie der Farne. Gustav Fischer, Jena (357 pp.).

Chumakov, N.M., Zharkov, M.A., 2002. Climate during Permian–Triassic biosphere reorganizations. Article 1: Climate of the Early Permian. Stratigr. Geol. Correl. 10, 586–602.

Cotta, B., 1832. Die Dendrolithen in Bezug auf ihren inneren Bau. Arnoldische Buchhandlung, Leipzig, Dresden (89 pp.).

Courty, M.A., Fédoroff, N., 1985. Micromorphology of recent and buried soils in a semi-arid region of northwestern India. Geoderma 35, 287–332.

Creber, G.T., Chaloner, W.G., 1984. Influence of environmental factors on the wood structure of living and fossil trees. Bot. Rev. 50, 357–448. http://dx.doi.org/10.1007/BF02862630.

Cridland, A.A., Morris, J.E., 1963. *Taeniopteris*, *Walchia*, and *Dichophyllum*, in the Pennsylvanian System of Kansas. Univ. Kans. Sci. Bull. 44, 71–85.

Dias-Brito, D., Rohn, R., Castro, J.C., Dias, R.R., Rößler, R., 2007. Floresta Petrificado do Tocantins Setentrional—O mais exuberante e importante registro florístico tropical–subtropical permiano no Hemisfério Sul. In: Winge, M., Schobbenhaus, C., Berbert-Born, M., Queiroz, E.T., Campos, D.A., Souza, C.R.G., Fernandes, A.C.S. (Eds.), Sítios Geológicos e Paleontológicos do Brasil. DNPM/CPRM—SIGEP, Brasilia (14 pp., Available online 23/01/2007 at http://www.unb.br/ig/sigep/sitio104/sitio104english.pdf).

Dietrich, D., Lampke, T., Rößler, R., 2013. A microstructure study on silicified wood from the Permian Petrified Forest of Chemnitz. Paläontol. Z. 87, 814–834. http://dx.doi.org/10.1007/s12542-012-0162-0.

DiMichele, W.A., 2014. Wetland–dryland vegetational dynamics in the Pennsylvanian ice age tropics. Int. J. Plant Sci. 175, 123–164.

DiMichele, W.A., Falcon-Lang, H.J., 2011. Pennsylvanian 'fossil forests' in growth position (T^0 assemblages): origin, taphonomic bias and palaeoecological insights. J. Geol. Soc. Lond. 168, 1–21.

DiMichele, W.A., Phillips, T.L., 1996. Climate change, plant extinctions and vegetational recovery during the Middle–Late Pennsylvanian Transition: the case of tropical peat-forming environments in North America. In: Hart, M.L. (Ed.), Biotic Recovery from Mass Extinctions. Geological Society London, Special Publication 102, pp. 201–221.

DiMichele, W.A., Phillips, T.L., Nelson, W.L., 2002. Place vs. time and vegetational persistence: a comparison of four tropical mires from the Illinois Basin during the height of the Pennsylvanian Ice Age. Int. J. Coal Geol. 50, 43–72.

DiMichele, W.A., Tabor, N.J., Chaney, D.S., Nelson, W.J., 2006. From wetlands to wet spots: environmental tracking and the fate of Carboniferous elements in Early Permian tropical floras. Geol. Soc. Am. Spec. Pap. 399, 223–248.

DiMichele, W.A., Chaney, D.S., Nelson, W.J., Lucas, S.G., Looy, C.V., Quick, K., Wang, J., 2007. A low diversity, seasonal tropical landscape dominated by conifers and peltasperms: Early Permian Abo Formation, New Mexico. Rev. Palaeobot. Palynol. 145, 249–273.

DiMichele, W.A., Kerp, H., Tabor, N.J., Looy, C.V., 2008. The so-called "Paleophytic–Mesophytic" transition in equatorial Pangea—multiple biomes and vegetational tracking of climate change through geological time. Palaeogeogr. Palaeoclimatol. Palaeoecol. 268, 152–163.

DiMichele, W.A., Montañez, I.P., Poulsen, C.J., Tabor, N.J., 2009. Climate and vegetational regime shifts in the late Paleozoic ice age earth. Geobiology 7, 200–226.

DiMichele, W.A., Cecil, C.B., Chaney, D.S., Elrick, S.D., Lucas, S.G., Lupia, R., Nelson, W.J., Tabor, N.J., 2011. Pennsylvanian–Permian vegetational changes in tropical Euramerica. In: Harper, J.A. (Ed.), Geology of the Pennsylvanian–Permian in the Dunkard basin: Guidebook, 76th Annual Field Conference of Pennsylvania Geologists, Washington DC, pp. 60–102.

Dunlop, J.A., Rößler, R., 2013. The youngest trigonotarbid, from the Permian of Chemnitz in Germany. Fossil Rec. 16, 229–243.

Eulenberger, S., Tunger, B., Fischer, F., 1995. Neue Erkenntnisse zur Geologie des Zeisigwaldes bei Chemnitz. Veröff. Mus. Naturkunde Chemnitz 18, 25–34.

Falcon-Lang, H.J., 1999. The Early Carboniferous (Courceyan–Arundian) monsoonal climate of the British Isles: evidence from growth rings in fossil woods. Geol. Mag. 136, 177–187.

Falcon-Lang, H.J., 2003. Growth interruptions in silicified conifer woods from the Upper Cretaceous Two Medicine Formation, Montana, USA: implications for palaeoclimate and dinosaur palaeoecology. Palaeogeogr. Palaeoclimatol. Palaeoecol. 199, 299–314.

Falcon-Lang, H.J., 2005. Intra-tree variability in wood anatomy and its implications for fossil wood systematic and palaeoclimatic studies. Palaeontology 48, 171–183.

Falcon-Lang, H.J., 2015. A calamitalean forest preserved in growth position in the Pennsylvanian coal measures of South Wales: implications for palaeoecology, ontogeny and taphonomy. Rev. Palaeobot. Palynol. 214, 51–67.

Falcon-Lang, H.J., Bashforth, A.R., 2004. Pennsylvanian uplands were forested by giant cordaitalean trees. Geology 32, 417–420. http://dx.doi.org/10.1130/G20371.1.

Falcon-Lang, H.J., Rygel, M.C., Calder, J.H., Gibling, M.R., 2004. An early Pennsylvanian waterhole deposit and its fossil biota in a dryland alluvial plain setting, Joggins, Nova Scotia. J. Geol. Soc. Lond. 161, 209–222.

Falcon-Lang, H.J., Nelson, W.J., Elrick, S., Looy, C.V., Ames, P.R., DiMichele, W.A., 2009. Incised channel fills containing conifers indicate that seasonally dry vegetation dominated Pennsylvanian tropical lowlands. Geology 37, 923–926.

Falcon-Lang, H.J., Jud, N.A., Nelson, W.J., DiMichele, W.A., Chaney, D.S., Lucas, S.G., 2011. Pennsylvanian coniferopsid forests in sabkha facies reveal the nature of seasonal tropical biome. Geology 39, 371–374. http://dx.doi.org/10.1130/G31764.1.

Fedo, C.M., Nesbitt, H.W., Young, G.M., 1995. Unraveling the effects of potassium metasomatism in sedimentary rocks and palaeosols, with implications for paleoweathering conditions and provenance. Geology 23, 921–924.

Feng, Z., Zierold, T., Rößler, R., 2012. When horsetails became giants. Chin. Sci. Bull. 57, 2285–2288.

Feng, Z., Rößler, R., Annacker, V., Yang, J.-Y., 2014. Micro-CT investigation of a seed fern (probable medullosan) fertile pinna from the Early Permian Petrified Forest in Chemnitz, Germany. Gondwana Res. 26, 1208–1215. http://dx.doi.org/10.1016/j.gr.2013.08.005.

Fischer, F., 1991. Das Rotliegende des ostthüringisch-westsächsischen Raumes (Vorerzgebirgs-Senke, Nordwestsächsischer Vulkanitkomplex, Geraer Becken). unpubl. PhD thesis, TU Bergakademie Freiberg.

Francis, J.E., 1984. The seasonal environment of the Purbeck (Upper Jurassic) fossil forests. Palaeogeogr. Palaeoclimatol. Palaeoecol. 48, 285–307.

Frenzel, D., 1759. Zuverlässige Nachricht von einem zu Steine gewordenen Baume, nebst dessen eigentlicher Abbildung. Dresdnisches Magazin 1. Michael Gröll, Dresden, pp. 39–47.

Galtier, J., Broutin, J., 2008. Floras from red beds of the Permian Basin of Lodève (Southern France). J. Iber. Geol. 34, 57–72.

Gastaldo, R.A., Stevanović-Walls, I.M., Ware, W.N., 2004. Erect forests are evidence for coseismic base-level changes in Pennsylvanian cyclothems of the Black Warrior Basin, USA. In: Pashin, J.C., Gastaldo, R.A. (Eds.), Sequence Stratigraphy, Paleoclimate, and Tectonics of Coal-bearing Strata. AAPG Studies in Geology 51, pp. 219–238.

Gile, L.H., Peterson, F.F., Grossman, R.B., 1966. Morphological and genetic sequences of carbonate accumulation in desert soils. Soil Sci. 101, 347–360.

Greb, S.F., Andrews, W.M., Eble, C.R., DiMichele, W.A., Cecil, C.B., Hower, J.C., 2003. Desmoinesian coal beds of the Eastern Interior and surrounding basins: the largest tropical peat mires in Earth history. In: Chan, M.A., Archer, A.W. (Eds.), Extreme depositional environments: mega end members in geologic time. Geological Society of America Special Papers 370, pp. 127–150.

Gulbranson, E.L., Montañez, I.P., Tabor, N.J., Limarino, O., 2015. Late Pennsylvanian aridification on the southwestern margin of Gondwana (Paganzo Basin, NW Argentina): a regional expression of a global climate perturbation. Palaeogeogr. Palaeoclimatol. Palaeoecol. 417, 220–235.

Harnois, L., 1988. The CIW index: a new chemical index of weathering. Sediment. Geol. 55, 319–322.

Hasiotis, S.T., Kraus, M.J., Demko, T.M., 2007. Climatic controls on continental trace fossils. In: Miller, W. (Ed.), Trace fossils: concepts, problems, prospects. Elsevier, pp. 172–195.

Hinz, J.K., Smith, I., Pfretzschner, H.-U., Wings, O., Sun, G., 2010. A high-resolution three-dimensional reconstruction of a fossil forest (Upper Jurassic, Shishugou Formation, Junggar Basin, Northwest China). Palaeodivers. Palaeoenviron. 90, 215–240.

Isbell, J.L., Henry, L.C., Gulbranson, E.L., Limarino, C.O., Fraiser, M.L., Koch, Z.J., Ciccioli, P.L., Dineen, A.A., 2012. Glacial paradoxes during the late Paleozoic ice age: evaluating the equilibrium line altitude as a control on glaciation. Gondwana Res. 22, 1–19.

Izart, A., Palhol, F., Gleixner, G., Elie, M., Blaise, T., Suarez-Ruiz, I., Sachsenhofer, R.F., Privalov, V.A., Panova, E.A., 2012. Palaeoclimate reconstruction from biomarker geochemistry and stable isotopes of n-alkanes from Carboniferous and Early Permian humic coals and limnic sediments in western and eastern Europe. Org. Geochem. 43, 125–149.

Jäger, F., 1939. Die Trockenseen der Erde. Petermanns Geographische Mitteilungen, Ergänzungsheft 236 (159 pp., Gotha).

Jenik, J., 1978. Roots and root systems in tropical trees: morphologic and ecologic aspects. In: Tomlinson, P.B., Zimmermann, M.H. (Eds.), Tropical Trees as Living Systems. Cambridge University Press, Cambridge, UK, pp. 323–349.

Jenny, H.J., 1941. Factors of Soil Formation. McGraw-Hill, New York (281 pp.).

Kerp, H., 1996. Post-Variscian late Palaeozoic Northern Hemisphere gymnosperms: the onset to the Mesozoic. Rev. Palaeobot. Palynol. 90, 263–285.

Kerp, H., 2000. The modernization of landscapes during the Late Paleozoic–Early Mesozoic. In: Gastaldo, R.A., DiMichele, W.A. (Eds.), Phanerozoic Terrestrial Ecosystems. Paleontological Society, New Haven, pp. 79–113.
Kerp, H., Fichter, J., 1985. Die Makrofloren des saarpfälzischen Rotliegenden (? Oberkarbon—Unter-Perm; SW-Deutschland). Mainz. Geowiss. Mitt. 14, 159–286.
Khadkikar, A.S., Merh, S.S., Malik, J.N., Camyal, L.S., 1998. Calcretes in semi-arid alluvial systems: formative pathways and sinks. Sediment. Geol. 116, 251–260.
Klappa, C.F., 1980. Rhizoliths in terrestrial carbonates: classification, recognition, genesis and significance. Sedimentology 27, 613–629.
Köppen, W., 1936. Das Geographisches System der Klimate. In: Köppen, W., Geiger, R. (Eds.), Handbuch der Klimatologie, Vol. 1 Part C. Gebrüder Borntraeger, Berlin, pp. 1–46.
Kraus, M.J., 1999. Paleosols in clastic sedimentary rocks: their geologic applications. Earth Sci. Rev. 47, 41–70.
Kraus, M.J., Hasiotis, S.T., 2006. Significance of different modes of rhizolith preservation to interpreting paleoenvironmental and paleohydrologic settings: examples from Paleogene paleosols, Bighorn Basin, Wyoming, U.S.A. J. Sediment. Res. 76, 633–646.
Kretzschmar, R., Annacker, V., Eulenberger, S., Tunger, B., Rößler, R., 2008. Erste wissenschaftliche Grabung im Versteinerten Wald von Chemnitz—ein Zwischenbericht. Freiberg. Forschungsh. C 528, 25–55.
Krings, M., Kerp, H., 2000. A contribution to the knowledge of the pteridosperm genera *Pseudomariopteris* Danzé-Corsin nov. emend. and *Helenopteris* nov. gen. Rev. Palaeobot. Palynol. 111, 145–195.
Kurzawe, F., Iannuzzi, R., Merlotti, S., Rößler, R., Noll, R., 2013a. New gymnospermous woods from the Permian of the Parnaíba Basin, northeastern Brazil, Part I: *Ductoabietoxylon*, *Scleroabietoxylon* and *Pamaiboxylon*. Rev. Palaeobot. Palynol. 195, 37–49. http://dx.doi.org/10.1016/j.revpalbo.2012.12.005.
Kurzawe, F., Iannuzzi, R., Merlotti, S., Rohn, R., 2013b. New gymnospermous woods from the Permian of the Parnaíba Basin, northeastern Brazil, Part II: *Damudoxylon*, *Kaokoxylon* and *Taeniopitys*. Rev. Palaeobot. Palynol. 195, 50–64. http://dx.doi.org/10.1016/j.revpalbo.2012.12.004.
Kutzbach, J.E., Ziegler, A.M., 1994. Simulation of Late Permian climate and biomes with an atmosphere–ocean model: comparisons with observations. In: Allen, J.R.L., Hoskins, B.J., Selwood, B.L., Spicer, R.A., Valdes, P.J. (Eds.), Palaeoclimates and their Modelling. With Special Reference to the Mesozoic Era. Chapman & Hall, London, pp. 119–132.
Legler, B., Schneider, J.W., 2008. Marine ingressions in context to one million years cyclicity of Permian red-beds (Upper Rotliegend II, Southern Permian Basin, Northern Germany). Palaeogeogr. Palaeoclimatol. Palaeoecol. 267, 102–114.
Looy, C.V., Kerp, H., Duijnstee, I.A.P., DiMichele, W.A., 2014. The late Paleozoic ecological–evolutionary laboratory, a land–plant fossil record perspective. Sediment. Rec. 12 (4), 4–10.
Lu, S., Wang, S., Chen, Y., 2015. Palaeopedogenesis of red palaeosols in Yunnan Plateau, southwestern China: pedogenical, geochemical and mineralogical evidences and palaeoenvironmental implication. Palaeogeogr. Palaeoclimatol. Palaeoecol. 420, 35–48.
Lützner, H.A., Schneider, J.W., Werneburg, R., 2012. Stefan und Rotliegend im Thüringer Wald und seiner Umgebung. In: Lützner, H., Kowalczyk, G. (Eds.), Stratigraphie von Deutschland. X. Rotliegend, Teil I: Innervariscische Becken. Schriftenreihe der Deutschen Gesellschaft für Geowissenschaften 61, pp. 418–487.
Machette, M.N., 1985. Calcic soils of the southwestern United States. Geol. Soc. Am. Spec. Pap. 203, 1–21.
Mack, G.H., James, W.C., 1994. Paleoclimate and the global distribution of paleosols. J. Geol. 102, 360–366.
Mack, G.H., James, W.C., Monger, H.C., 1993. Classification of paleosols. Geol. Soc. Am. Bull. 305, 129–136.
Mack, G.H., Cole, D.R., Trevino, L., 2000. The distribution and discrimination of shallow, authigenic carbonate in the Pliocene–Pleistocene Palomas Basin, southern Rio Grande rift. Geol. Soc. Am. Bull. 112, 643–656.
Mack, G.H., Tabor, N.J., Zollinger, H.J., 2010. Palaeosols and sequence stratigraphy of the Lower Permian Abo Member, south-central New Mexico, USA. Sedimentology 57, 1566–1583.
Matysová, P., Rössler, R., Götze, J., Leichmann, J., Forbes, G., Taylor, E.L., Sakala, J., Grygar, T., 2010. Alluvial and volcanic pathways to silicified plant stems (Upper Carboniferous–Triassic) and their taphonomic and palaeoenvironmental meaning. Palaeogeogr. Palaeoclimatol. Palaeoecol. 292, 127–143.
McLennan, S.M., 1993. Weathering and global denudation. J. Geol. 101, 295–303. http://dx.doi.org/10.1086/648222.
Montañez, I.P., Poulsen, C.J., 2013. The Late Paleozoic Ice Age: an evolving paradigm. Annu. Rev. Earth Planet. Sci. 41, 629–656.
Nash, D.J., Ullyott, J.S., 2007. Silcrete. In: Nash, D.J., McLaren, S.J. (Eds.), Geochemical Sediments and Landscapes. Blackwell Publishing, Oxford (465 pp.).
Nash, D.J., McLaren, S.J., Webb, J.A., 2004. Petrology, geochemistry and environmental significance of silcrete–calcrete intergrade duricrusts at Kang Pan and Tswaane, Central Kalahari, Botswana. Earth Surf. Process. Landf. 29, 1559–1586.
Neregato, R., Rößler, R., Rohn, R., Noll, R., 2015. New petrified calamitaleans from the Permian of the Parnaíba Basin, central-north Brazil. Part I. Rev. Palaeobot. Palynol. 215, 23–45.
Nesbitt, H.W., Young, G.M., 1982. Early Proterozoic climates and plate motions inferred from mayor element chemistry of lutites. Nature 299, 715–717. http://dx.doi.org/10.1038/299715a0.
Nordt, L.C., Driese, S.D., 2010. New weathering index improves paleorainfall estimates from vertisols. Geology 38, 407–410.
Nordt, L., Orosz, M., Driese, S., Tubbs, J., 2006. Vertisol carbonate properties in relation to mean annual precipitation: implications for paleoprecipitation estimates. J. Geol. 114, 501–510.
Opluštil, S., Pšenička, J., Libertín, M., Šimůnek, Z., 2007. Vegetation patterns of Westphalian and Lower Stephanian mire assemblages preserved in tuff beds of the continental basins of Czech Republic. Rev. Palaeobot. Palynol. 143, 107–154.
Opluštil, S., Pšenička, J., Libertín, M., Bek, J., Daňková, J., Šimunek, Z., Drabkova, J., 2009. Composition and structure of an in situ Middle Pennsylvanian peat-forming plant assemblage in volcanic ash, Radnice Basin (Czech Republic). Palaios 24, 726–746.
Opluštil, S., Pšenička, J., Bek, J., Wang, J., Feng, Z., Libertín, M., Šimunek, Z., Bureš, J., Drábková, J., 2014. T^0 peat-forming plant assemblage preserved in growth position by volcanic ash-fall: a case study from the Middle Pennsylvanian of the Czech Republic. Bull. Geosci. 1499, 773–818 (doi 10.3140).
Peyser, C.E., Poulsen, C.J., 2008. Controls on Permo-Carboniferous precipitation over tropical Pangaea: a GCM sensitivity study. Palaeogeogr. Palaeoclimatol. Palaeoecol. 268, 181–192.
Pfefferkorn, H.W., 1980. A note on the term "Upland flora". Rev. Palaeobot. Palynol. 30, 157–158.
Pfefferkorn, H.W., Fuchs, K., 1991. A field classification of fossil plant substrate interactions. Neues Jb. Geol. Paläontol. Abh. 183, 17–36.
Pfefferkorn, H.W., Gastaldo, R.A., DiMichele, W.A., Phillips, T.L., 2008. Pennsylvanian tropical floras from the United States as a record of changing climate. In: Fielding, C.R., Frank, T.D., Isbell, J.L. (Eds.), Resolving the Late Paleozoic Ice Age in Time and Space. Geological Society of America Special Papers 441, pp. 305–316.
Pimentel, N.L., Wright, V.P., Azevedo, T.M., 1996. Distinguishing early groundwater alteration effects pedogenesis in ancient alluvial basins: examples from the Palaeogene of southern Portugal. Sediment. Geol. 105, 1–10.
PiPujol, M.D., Buurman, P., 1994. The distinction between ground-water gley and surface-water gley phenomena in Tertiary paleosols of the Ebro basin, NE Spain. Palaeogeogr. Palaeoclimatol. Palaeoecol. 110, 103–113.
PiPujol, M.D., Buurman, P., 1997. Dynamics of iron and calcium carbonate redistribution and paleohydrology in middle Eocene alluvial paleosols of the southeast Ebro Basin margin (Catalonia, northeast Spain). Palaeogeogr. Palaeoclimatol. Palaeoecol. 134, 87–107.
Purvis, K., Wright, V.P., 1991. Calcretes related to phreatophytic vegetation from the Middle Triassic Otter Sandstone of South West England. Sedimentology 38, 539–551.
Raymond, A., Wehner, M., Costanza, S.H., 2014. Permineralized *Alethopteris ambigua* (Lesquereux) White: a medullosan with relatively long-lived leaves, adapted for sunny habitats in mires and floodplains. Rev. Palaeobot. Palynol. 200, 82–96.
Retallack, G.J., 1988. Field recognition of paleosols. In: Reinhardt, J., Sigleo, W.R. (Eds.), Paleosols and weathering through geologic time: principles and applications. Geological Society of America Special Papers 216, pp. 1–20.
Retallack, G.J., 1991. Miocene Paleosols and Ape Habitats in Pakistan and Kenya. Oxford University Press, New York (246 pp.).
Retallack, G.J., 1994. The environmental factor approach to the interpretation of paleosols. In: Amundson, R., Harden, J., Singer, M. (Eds.), Factors of Soil Formation: A fiftieth Anniversary Retrospective (Chapter 3). Soil Science Society of America Special Publications 33, pp. 31–64.
Retallack, G.J., 1999. Paleosols. In: Jones, T.P., Rowe, N.P. (Eds.), Fossil plants and spores: modern techniques. The Geological Society, London, pp. 214–219.
Retallack, G.J., 2000. Depth to pedogenic carbonate horizon as a palaeoprecipitation indicator? Comment and reply: comment. Geology 28, 572.
Retallack, G.J., 2001. Soils of the Past. An Introduction to Paleopedology. 2nd ed. Blackwell, Oxford (404 pp.).
Retallack, G.J., 2005. Pedogenic carbonate proxies for amount and seasonality of precipitation in paleosols. Geology 33, 333–336. http://dx.doi.org/10.1130/G21263.1.
Retallack, G.J., Huang, C., 2010. Depth to gypsic horizon as a proxy for paleoprecipitation in paleosols of sedimentary environments. Geology 38 (5), 403–406.
Ricardi-Branco, F., 2008. Venezuelan paleoflora of the Pennsylvanian–Early Permian: paleobiogeographical relationships to central and western equatorial Pangea. Gondwana Res. 14, 297–305.
Richter, H.G., Grosser, D., Heinz, I., Gasson, P.E., 2004. IAWA list of microscopic features for softwood identification. IAWA J. 25, 1–70.
Roscher, M., Schneider, J.W., 2005. An annotated correlation chart for continental Late Pennsylvanian and Permian basins and the marine scale. In: Lucas, S.G., Zeigler, K.E. (Eds.), The Nonmarine Permian. New Mexico Museum of Natural History and Science Bulletin 30, pp. 282–291.
Roscher, M., Schneider, J.W., 2006. Permocarboniferous climate: Early Pennsylvanian to Late Permian climate development of central Europe in a regional and global context. In: Lucas, S.G., Cassinis, G., Schneider, J.W. (Eds.), Non Marine Permian Chronology and Correlation. Geological Society London, Special Publication 265, pp. 5–136.
Roscher, M., Berner, U., Schneider, J.W., 2008. Climate modelling—a tool for the assessment of the palaeo-distribution of source and reservoir rocks. Oil Gas Eur. Mag. 3, 131–137.
Roscher, M., Stordal, F., Svensen, H., 2011. The effect of global warming and global cooling on the distribution of the latest Permian climate zones. Palaeogeogr. Palaeoclimatol. Palaeoecol. 309, 186–200.
Rosenau, N.A., Tabor, N.J., Elrick, S.D., Nelson, W.J., 2013. Polygenetic history of paleosols In Middle–Upper Pennsylvanian cyclothems of the Illinois Basin, USA: Part II. Integrating geomorphology, climate, and glacioeustasy. J. Sediment. Res. 83, 637–668.
Rößler, R., 2000. The late Palaeozoic tree fern *Psaronius*—an ecosystem unto itself. Rev. Palaeobot. Palynol. 108, 55–74.
Rößler, R., 2006. Two remarkable Permian petrified forests: correlation, comparison and significance. In: Lucas, S.G., Cassinis, G., Schneider, J.W. (Eds.), Non-Marine Permian

Biostratigraphy and Biochronology. Geological Society London, Special Publication 265, pp. 39–63.
Rößler, R., Galtier, J., 2002a. First *Grammatopteris* tree fern from the Southern Hemisphere—new insights in the evolution of the Osmundaceae from the Permian of Brazil. Rev. Palaeobot. Palynol. 121, 205–230.
Rößler, R., Galtier, J., 2002b. *Dernbachia brasiliensis* gen. nov. et sp. nov.—a new small tree fern from the Permian of NE Brazil. Rev. Palaeobot. Palynol. 122, 239–263.
Rößler, R., Galtier, J., 2003. The first evidence of the fern *Botryopteris* from the Permian of the Southern Hemisphere reflecting growth form diversity. Rev. Palaeobot. Palynol. 127, 99–124.
Rößler, R., Merbitz, M., 2009. Fenster in die Erdgeschichte—Die Suche nach Kieselhölzern auf dem Sonnenberg in Chemnitz. Veröff. Mus. Naturkunde Chemnitz 32, 47–54.
Rößler, R., Noll, R., 2006. Sphenopsids of the Permian (I): the largest known anatomically preserved calamite, an exceptional find from the petrified forest of Chemnitz, Germany. Rev. Palaeobot. Palynol. 140, 145–162.
Rößler, R., Noll, R., 2007. *Calamitea* Cotta, the correct name for calamitean sphenopsids currently classified as *Calamodendron* Brongniart. Rev. Palaeobot. Palynol. 144, 157–180.
Rößler, R., Noll, R., 2010. Anatomy and branching of *Arthropitys bistriata* (Cotta) Goeppert—new observations from the Permian petrified forest of Chemnitz, Germany. Int. J. Coal Geol. 83, 103–124.
Rößler, R., Annacker, V., Kretzschmar, R., Eulenberger, S., Tunger, B., 2008. Auf Schatzsuche in Chemnitz—Wissenschaftliche Grabungen '08. Veröff. Mus. Naturkunde Chemnitz 31, 5–44.
Rößler, R., Kretzschmar, R., Annacker, V., Mehlhorn, S., 2009. Auf Schatzsuche in Chemnitz—Wissenschaftliche Grabungen ,'09. Veröff. Mus. Naturkunde Chemnitz 32, 25–46.
Rößler, R., Kretzschmar, R., Annacker, V., Mehlhorn, S., Merbitz, M., Schneider, J.W., Luthardt, L., 2010. Auf Schatzsuche in Chemnitz—Wissenschaftliche Grabungen '10. Veröff. Mus. Naturkunde Chemnitz 33, 27–50.
Rößler, R., Feng, Z., Noll, R., 2012a. The largest calamite and its growth architecture—*Arthropitys bistriata* from the Permian petrified forest of Chemnitz. Rev. Palaeobot. Palynol. 185, 64–78.
Rößler, R., Zierold, T., Feng, Z., Kretzschmar, R., Merbitz, M., Annacker, V., Schneider, J.W., 2012b. A snapshot of an Early Permian ecosystem preserved by explosive volcanism: new results from the petrified forest of Chemnitz, Germany. Palaois 27, 814–834.
Rößler, R., Merbitz, M., Annacker, V., Luthardt, L., Noll, R., Neregato, R., Rohn, R., 2014. The root systems of Permian arborescent sphenopsids: evidence from the Northern and Southern hemispheres. Palaeontogr. B 291 (4–6), 65–107.
Royer, D.L., 1999. Depth to pedogenic carbonate horizon as a palaeoprecipitation indicator? Geology 27, 1123–1126.
Ruxton, B.P., 1968. Measures of the degree of chemical weathering of rocks. J. Geol. 76, 518–527.
Sahney, S., Benton, M.J., Falcon-Lang, H.J., 2010. Rainforest collapse triggered Carboniferous tetrapod diversification in Euramerica. Geology 38, 1079–1082.
Schneider, J.W., 1994. Environment, biotas and taphonomy of the Lower Permian lacustrine Niederhäslich limestone, Döhlen-basin, Germany. Trans. R. Soc. Edinb. Earth Sci. 84, 453–464.
Schneider, J.W., Gebhardt, U., 1993. Litho- und Biofaziesmuster in intra- und extramontanen Senken des Rotliegend (Perm, Nord- und Ostdeutschland). Geol. Jahrb. A 131, 57–98.
Schneider, J.W., Romer, R.L., 2010. The Late Variscan Molasses (Late Carboniferous to Late Permian) of the Saxo-Thuringian Zone. In: Linnemann, U., Romer, R.L. (Eds.), Pre-Mesozoic Geology of Saxo-Thuringia—From the Cadomian Active Margin to the Variscan Orogen. Schweizerbart Science Publishers, Stuttgart, pp. 323–346.
Schneider, J.W., Rößler, R., 1995. Permische Calcisol-Paläoböden mit Rhizolithen und Wirbeltierresten—Sedimentation, Lebewelt und Klimaentwicklung im Rotliegend der Härtensdorf-Formation (Erzgebirge-Becken). Veröff. Mus. Naturkunde Chemnitz 18, 53–70.
Schneider, J.W., Werneburg, R., 2012. Biostratigraphie des Rotliegend mit Insekten und Amphibien. In: Lützner, H., Kowalczyk, G. (Eds.), Stratigraphie von Deutschland X. Rotliegend. Teil I: Innervariscische Becken. Schriftenreihe der Deutschen Gesellschaft für Geowissenschaften 61, pp. 110–142.
Schneider, J.W., Siegesmund, S., Gebhardt, U., 1984. Paläontologie und Genese limnischer Schill- und Algenkarbonate in der Randfazies der kohleführenden Wettiner Schichten (Oberkarbon, Stefan C) des NE-Saaletroges. Hallesches Jb. Geowiss. 9, 35–51.
Schneider, J.W., Körner, F., Roscher, M., Kroner, V., 2006. Permian climate development in the northern peri-Tethys—the Lodève basin, French Massif Central, compared in a European and global context. Palaeogeogr. Palaeoclimatol. Palaeoecol. 240, 161–183.
Schneider, J.W., Lucas, S.G., Werneburg, R., Rößler, R., 2010. Euramerican Late Pennsylvanian/Early Permian arthropleurid/tetrapod associations—implications for the habitat and paleobiology of the largest terrestrial arthropod. In: Lucas, S.G., Schneider, J.W., Spielmann, J.A. (Eds.), Carboniferous–Permian transition in Cañon del Cobre, northern New Mexico. New Mexico Museum of Natural History and Science, Bulletin 49, pp. 49–70.
Schneider, J.W., Rößler, R., Fischer, F., 2012. Rotliegend des Chemnitz-Beckens (syn. Erzgebirge-Becken). In: Lützner, H., Kowalczyk, G. (Eds.), Stratigraphie von Deutschland. X. Rotliegend. Teil I: Innervariscische Becken. Schriftenreihe der Deutschen Gesellschaft für Geowissenschaften 61, pp. 530–588.
Schneider, J.W., Lucas, S.G., Barrick, J., Werneburg, R., Shcherbakov, D.E., Silantev, V., Shen, S., Saber, H., Belahmira, A., Scholze, F., Rößler, R., 2014. Carboniferous and Permian nonmarine–marine correlation—methods, results, future tasks. In: Nurgaliev, D.K., Silantiev, V.V., Urazaeva, M.N. (Eds.), Kazan Golovkinsky Stratigraphic Meeting, 2014. Carboniferous and Permian Earth systems, stratigraphic events, biotic evolution, sedimentary basins and resources. October, 20–23, Kazan, Russia. Abstract Volume.—Kazan Federal University. Institute of geology and petroleum technologies, Kazan, pp. 73–77.
Schweingruber, F.H., Börner, A., Schulze, E.-D., 2008. Atlas of Woody Plant Stems—Evolution, Structure and Environmental Modifications. Springer, Heidelberg, Berlin http://dx.doi.org/10.1007/978-3-540-32525-3 (229 pp.).
Schweingruber, F.H., Börner, A., Schulze, E.-D., 2011. Atlas of Stem Anatomy in Herbs, Shrubs and Trees. Springer, Berlin, Heidelberg (495 pp.).
Sehgal, J.L., Stoops, G., 1972. Pedogenic calcite accumulation in arid and semi-arid regions of the Indo-Gangetic alluvial plain Erstwhile Punjab (India)—their morphology and origin. Geoderma 8, 59–72.
Semeniuk, V., Meagher, T.D., 1981. Calcrete in Quarternary coastal dunes in southeastern Australia: a capillary-rise phenomenon associated with plants. J. Sediment. Petrol. 51, 47–68.
Shao, J.Q., Yang, S.Y., 2012. Does chemical index of alteration (CIA) reflect silicate weathering and monsoonal climate in the Changjiang River basin? Chin. Sci. Bull. 57, 1178–1187. http://dx.doi.org/10.1007/s11434-011-4954-5.
Sheldon, N.D., Retallack, G.J., 2001. Equation for compaction of paleosols due to burial. Geology 29, 247–250.
Sheldon, N.D., Tabor, N.J., 2009. Quantitative paleoenvironmental and paleoclimatic reconstruction using paleosols. Earth Sci. Rev. 95, 1–52.
Sheldon, N.D., Retallack, G.J., Tanaka, S., 2002. Geochemical climofunctions from North America soils and application to paleosols across the Eocene–Oligocene boundary in Oregon. J. Geol. 110, 687–696.
Singh, K.P., Singh, R.P., 1981. Seasonal variations in biomass and energy of small roots in a tropical dry forest. Oikos 37, 88–92.
Spötl, C., Wright, V.P., 1992. Groundwater dolocretes from the Upper Triassic of the Paris Basin, France: a case study of an arid, continental diagenetic facies. Sedimentology 39, 1119–1136.
Sterzel, J.T., 1875. Die fossilen Pflanzen des Rothliegenden von Chemnitz in der Geschichte der Paläontologie. Ber. Naturwiss. Ges. Chemnitz 5, 71–243.
Sterzel, J.T., 1904. Ein verkieselter Riesenbaum aus dem Rotliegenden von Chemnitz. Ber. Naturwiss. Ges. Chemnitz 15, 23–41.
Sterzel, J.T., 1918. Die organischen Reste des Kulms und des Rotliegenden der Gegend von Chemnitz: Abhandlungen der Königlich Sächsischen Gesellschaft der Wissenschaften. Math.-Phys. Kl. 35 (5), 205–315.
Stiles, C.A., Mora, C.I., Driese, S.G., 2001. Pedogenic iron–manganese nodules in Vertisols: a new proxy for paleoprecipitation? Geology 29, 943–946.
Stworzewicz, E., Szulc, J., Pokryszko, B.M., 2009. Late Paleozoic continental gastropods from Poland: systematic, evolutionary and paleoecological approach. J. Paleontol. 83, 938–945.
Tabor, N.J., 2013. Wastelands of tropical Pangea: high heat in the Permian. Geology 41, 623–624.
Tabor, N.J., Montañez, I.P., 2005. Oxygen and hydrogen isotope compositions of Permian pedogenic phyllsilicates: development of modern surface domain arrays and implications for paleotemperature reconstructions. Palaeogeogr. Palaeoclimatol. Palaeoecol. 223, 127–146.
Tabor, N.J., Poulsen, C.J., 2008. Palaeoclimate across the Late Pennsylvanian–Early Permian tropical palaeolatitudes: a review of climate indicators, their distribution, and relation to palaeophysiographic climate factors. Palaeogeogr. Palaeoclimatol. Palaeoecol. 268, 293–310.
Tabor, N.J., Smith, R.M.H., Steyer, S., Sidor, C.A., Poulsen, C.J., 2011. The Permian Moradi Formation of northern Niger: paleosol morphology, petrography and mineralogy. Palaeogeogr. Palaeoclimatol. Palaeoecol. 299, 200–213.
Tavares, T.M.V., Rohn, R., Rößler, R., Noll, R., 2014. Petrified Marattiales pinnae from the Lower Permian of North-Western Gondwana (Parnaíba Basin, Brazil). Rev. Palaeobot. Palynol. 201, 12–28. http://dx.doi.org/10.1016/j.revpalbo.2013.09.002.
Taylor, T.N., Taylor, E.L., Krings, M., 2009. Paleobotany—The Biology and Evolution of Fossil Plants. 2nd edition. Elsevier and Academic Press, Amsterdam (1230 pp.).
Thiry, M., Milnes, A.R., 1991. Pedogenic and groundwater silcretes at Stuart Creek opal field, South Australia. J. Sediment. Petrol. 61, 111–127.
Torsvik, T.H., Cocks, L.R.M., 2004. Earth geography from 400 to 250 Ma: a palaeomagnetic, faunal and facies review. J. Geol. Soc. Lond. 161, 555–572. http://dx.doi.org/10.1144/0016-764903-098.
Vacca, A., Ferrara, C., Matteucci, R., Murru, M., 2012. Ferruginous paleosols around the Cretaceous–Paleocene boundary in central-southern Sardinia (Italy) and their potential as pedostratigraphic markers. Quat. Int. 265, 179–190.
Wagner, R.H., 1989. A late Stephanian forest swamp with *Sporangiostrobus* fossilized by volcanic ash fall in the Puertollano Basin, central Spain. Int. J. Coal Geol. 12, 523–552.
Wagner, S., Günster, N., Skowronek, A., 2012. Genesis and climatic interpretation of paleosols and calcretes in a plio-pleistocene alluvial fan of the costa blanca (SE Spain). Quat. Int. 265, 170–178.
Wang, J., Pfefferkorn, H.W., Zhang, Y., Feng, Z., 2012. Permian vegetational Pompeii from Inner Mongolia and its implications for landscape paleoecology and paleobiogeography of Cathaysia. Proc. Natl. Acad. Sci. U. S. A. 109, 4927–4932.
Wang, J., Kerp, H., Pfefferkorn, H.W., 2014. The earliest occurrence of peltasperms in the basal Permian strata of the North China Block and the radiation of this group. Geol. J. 49, 129–142.
Watts, N.L., 1978. Displacive calcite: evidence from recent and ancient calcretes. Geology 6, 699–703.
Watts, N.L., 1980. Quaternary pedogenic calcretes from the Kalahari (southern Africa): mineralogy, genesis and diagenesis. Sedimentology 27, 661–686.
Wheeler, E., Baas, P., Gasson, P.E., 1989. IAWA list of microscopic features for hardwood identification. IAWA Bull. 10, 219–332.

Wheeler, E.A., Wiemann, M.C., Fleagle, J.G., 2007. Woods from the Miocene Bakate Formation, Ethiopia—anatomical characteristics, estimates of original specific gravity and ecological inferences. Rev. Palaeobot. Palynol. 146, 193–207. http://dx.doi.org/10.1016/j.revpalbo.2007.04.002.

Widdowson, M., 2007. Laterite und Ferricrete. In: Nash, D.J., McLaren, S.J. (Eds.), Geochemical Sediments and Landscapes. Blackwell Publishing, Oxford, pp. 46–94.

Wittke, K., Götze, J., Rößler, R., Dietrich, D., Marx, G., 2004. Raman and cathodoluminescence spectroscopic investigations on Permian fossil wood from Chemnitz: a contribution to the study of the permineralization process. Spectrochim. Acta A 60, 2903–2912.

Wright, V.P., 1987. The ecology of two early Carboniferous paleosols. In: Miller, J., Adams, A.E., Wright, V.P. (Eds.), European Dinantian Environments. Geological Journal Special Issue 12, pp. 345–358.

Wright, V.P., 1992. Paleopedology: stratigraphic relationships and empirical models. In: Martini, I.P., Chesworth, W. (Eds.), Weathering, Soils and Paleosols. Developments in Earth Surface Processes 2, pp. 475–500.

Wright, V.P., 2007. Calcrete. In: McLaren, S.J., Nash, D.J. (Eds.), Geochemical Sediments and Landscapes. Blackwell Publishing, pp. 10–45.